Modelling Shade-Intolerant Tree Responses to Forest Edges

By

Kara-Lyne Shaw

A Thesis Submitted to Saint Mary's University, Halifax, Nova Scotia in Partial Fulfillment of the Requirements for the Degree of Master of Science in Applied Science.

Approved: Dr. Karen Harper
Supervisor
Department of Biology
Saint Mary's University

Approved: Dr. Paul Muir
Supervisor
Department of Mathematics and Computer Science
Saint Mary's University

Approved: Dr. Élise Filotas
External Examiner
Département de Science et technologie
TÉLUQ — Université du Québec

Approved: Dr. Steve Cumming
Supervisory Committee Member
Département des sciences du bois et de la forêt
Université Laval

Approved: Dr. Philip Giles
Supervisory Committee Member
Department of Geography and Environmental Studies
Saint Mary's University

September 14th, 2023

Abstract

Modelling Shade-Intolerant Tree Responses to Forest Edges

By

Kara-Lyne Shaw

September 14th, 2023

Abstract: Amidst growing global forest fragmentation, understanding the impacts of edges on forest ecosystems has become increasingly important for researchers and conservationists. However, the expanding scope of edge creation highlights the limitations of field studies. Models offer an accessible means to simulate edge effects in a time and cost effective manner. This thesis explores the potential of ordinary differential equation (ODE) models to describe simulated vegetation responses of shade-intolerant trees following the establishment of a clear-cut edge in a boreal ecosystem. Through time-dependent parameters, I developed a suite of nested models capturing observable population trends in seedlings, saplings, and adult shade-intolerant trees. Sensitivity analyses were conducted to assess model robustness and predictive capability. This research will contribute to future implementations of edge vegetation response models, aiming to enhance our understanding of the long-term effects of edge creation.

Contents

List of Figures

List of Tables

Chapter 1

Introduction

1.1 Background

Approximately 70% of remaining forested area on Earth is within 1 km of a forest edge (Haddad et al., 2015). As global forest fragmentation continues to increase, there has been remarkable effort put forth by edge researchers to better understand the impacts of edge creation. Over the previous three decades, there has been a significant increase in the number of studies on vegetation responses at forest edges (Franklin et al., 2021). Such studies explore how edge creation influences interior forests given a variety of factors such as the origin of edge creation, forest type, and geographical location (Ries et al., 2004).

Forest edges, as defined by Franklin et al. (2021), are the transitional areas between forested and nonforested regions that play a critical role in shaping landscapes. As the edge of a forest is often ecologically distinct from adjacent patches, understanding the underlying system dynamics and ecological patterns of habitats near the edge is integral to understanding the impacts of habitat fragmentation (Ries et al., 2004). The presence of a forest edge has the potential to strongly influence adjacent ecological

systems (Harper et al., 2005). Edge influence describes the detectable differences in community structure, composition, and function between the edge and interior forest (Murcia, 1995; Ruffell & Didham, 2016; Harper et al., 2005). Edge creation can elicit diverse habitat responses, encompassing abiotic factors like temperature and humidity, as well as biological aspects like species abundance and distribution (Murcia, 1995; Didham & Lawton, 1999; Laurance et al., 2002).

1.2 Forest Edge Types

Forest edges are classified as either the result of a disturbance or inherent features of the landscape (Franklin et al., 2021). Thomas et al. (1979) describe the presence of inherent edges within a landscape as attributed to geomorphic conditions or various other factors, and consider them to be integral components of the overall terrain. Edges created as a result of a disturbance are classified as either natural or anthropogenic edges. Anthropogenic edges are edges created as a result of anthropogenic influence such as forest harvesting, agricultural development, or roads (Franklin et al., 2021). Natural edges however, are defined by Franklin et al. (2021) as the result of a natural phenomena such as wildfires or insect outbreaks.

Franklin et al. (2021) found that a vast majority of edge studies focus on anthropogenic edges. However, natural edges also exhibit distinct vegetation patterns when compared to neighbouring patches and should be considered for further exploration. As such, the results of this synthesis suggested that both anthropogenic and natural edges are dynamic features of fragmented landscapes, indicating a further need for empirical studies for both edge types.

Edges established as a result of a disturbance often alter the ecosystem dynamics of neighbouring habitats (Franklin et al., 2021). Disturbance edges have the potential

to alter the microclimate conditions of its neighbouring patches (Harper et al., 2005). Increased exposure levels of factors such as sunlight, wind, and temperature variations can lead to changes in moisture levels, temperature gradients, and light availability (Braithwaite & Mallik, 2012; Hofmeister et al., 2019). Chen et al. (1992) found that these changes may lead to increased seedling establishment and plant growth at edge communities. Created edges alter the flow of organisms, energy, and materials between adjacent systems (Ries et al., 2004; Schtickzelle & Baguette, 2003). Likewise, disturbance edges influence interactions among species such as the spread of pathogens, pollination, seed dispersal, and herbivory, altering overall biodiversity (Murcia, 1995; Didham et al., 2012). Turner et al. (1993) defined disturbance edges as catalysts for a cascade of ecological processes, including secondary succession, patch dynamics, and landscape connectivity, with far-reaching implications for broader-scale ecological phenomena such as dispersal patterns, gene flow, and metapopulation dynamics.

Haddad et al. (2015) define anthropogenically-induced edges as the result of human-transformed land cover (e.g., roads, crops, pastures, etc.). As global forest fragmentation continues to increase, the findings of this synthesis suggest that understanding the effects caused by various anthropogenic edge types is becoming increasingly critical. However, edges resulting from natural disturbances such as wildfires or insect outbreaks, as mentioned earlier, also influence habitat conditions (Franklin et al., 2021). The vegetation responses resulting from disturbance-related edges vary between anthropogenic and natural influence. For instance, Harper et al. (2015) report that edge influence on vegetation responses of boreal forests is less extensive at cut edges when compared to that of fire edges. However, for biomes with high levels of biomass such as temperate and tropical forests, edge influence tends to be more considerable (Harper et

al., 2005; McWethy et al., 2009). For anthropogenic edges in temperate forests, studies reported an increase in biomass with negligible changes to tree mortality near the edge when compared to the adjacent interior systems (Wales, 1972; Reinmann & Hutyra, 2017). For natural edges however, temperate forests displayed increased biodiversity and species diversity in communities located at the edge (Esseen et al., 2016; Poepperl & Seidl, 2021; Thom et al., 2017), but responses such as an increase in dead wood were also observed near the edge (Wales, 1972; Poepperl & Seidl, 2021). Franklin et al. (2021) found that tropical forests tend to display the most extreme vegetation responses to anthropogenic edge creation, with observable edge influence as extensive as 500 m for some tropical systems. However, when compared to temperate and boreal forests, this synthesis found that studies regarding naturally-induced tropical edges are generally sparse in the literature.

Clear-cut harvesting, otherwise known as clear-cutting, is a method of timber harvesting involving the removal of all trees within a designated area (Keenan & Kimmins, 1993). Keenan & Kimmins (1993) describe this method as the harvest of all trees from the stand regardless of age, species, or size. The result of this form of harvest is the complete removal of the forest canopy, leaving the area devoid of standing trees. The sudden removal of an entire portion of a forest often has significant and long-lasting effects on the adjacent ecosystem (Haddad et al., 2015). Keenan & Kimmins (1993) found that shade-intolerant tree populations play a pioneering role in the early successional stages post clear-cut. For shade-intolerant tree populations, the study found that clear-cutting creates an opportunity for seedling establishment given the newly-opened canopy. Furthermore, reduced competition at the edge promotes increased growth rates in shade-intolerant tree populations, leading to a distinct species com-

position favouring shade-intolerant species over shade-tolerant ones. Nevertheless, as the canopy gradually re-establishes, the study's findings suggest that there may be a compositional shift back to shade-tolerant species.

1.3 Edge Models

Edge models have been implemented and used by edge researchers to better understand the factors that drive edge influence on interior systems (Ries & Sisk, 2004). Many edge models specialize in evaluating how specific factors impact edge influence. For instance, the logistic regression models constructed by Mitchell et al. (2001) predict windthrow damage that often occurs along clear-cut boundaries on northern Vancouver Island. However, less specific models are also available to allow for flexibility in the simulation design and consideration of influential factors. For example, the SORTIE-ND model (Canham, n.d.), discussed in greater detail later in this thesis, offers users the ability to implement and manipulate diverse forest types, enabling researchers to assess a wide array of edge variations.

Menard et al. (2002) state that the implementation of edge models varies greatly, with many such models using combinations of stochastic and deterministic processes to define complex forest simulations under varying conditions. They describe these models to implement stochastic and deterministic processes through complex simulation and validation procedures, capable of producing intricate and interrelated representations of forest systems. Menard et al. (2002) found that many of these models, referred to as successional models, are derived from the JABOWA model for specific applications in different ecosystems. The JABOWA model, initially released in 1972, holds a notable place as one of the earliest process-based individual tree models (Botkin, 1993). Since the creation of the JABOWA model, it has served as the predecessor for

a family of over 60 variant process-based models (Ashraf et al., 2012). As summarized by Ewers & Didham (2006), these models are capable of describing complex vegetation responses across habitat boundaries, these responses can be verified through data collection. These models become especially important when it comes to predicting and evaluating edge influence over a significant period of time.

1.4 Research Gaps and Motivation

Franklin et al. (2021) stated that boreal forests are generally characterized by their relatively weak extent of edge influence on vegetation. This can be attributed to the frequent occurrence of natural disturbances and the significant heterogeneity in forest structure and composition (Harper & Macdonald, 2002). Following this realization, the synthesis by Franklin et al. (2021) discovered that the majority of available edge studies on boreal forests have focused on fire, insect outbreak, and young-harvest edges. However, there is a lack of studies on the long-term edge effects of *Populus*-dominated mixed-wood boreal forests post clear-cut. *Populus*-dominated mixed-wood forests are ecologically significant given their biodiversity (Anyomi et al., 2022), ecological resilience (Anyomi et al., 2022), carbon sequestering properties (Payne, 2019), and economic value (Richardson et al., 2007). The study conducted by Harper & Macdonald (2002) on the spatial and temporal patterns of edge influence following harvesting in *Populus tremuloides*-dominated boreal mixed-wood forests identified changes in understorey abundance and species composition as more significant in older edges than that of younger edges. Given the results of this study, a temporal evaluation of population responses of shade-intolerant trees post-harvest may provide clearer insights into the long-term edge effects of clear-cut harvesting. A model capable of describing these responses could provide a method in which to further compare shade-intolerant

tree responses for different edge and forest types.

1.5 Objectives and Significance

I investigated the use of mathematical models to bridge the research gap between current edge studies and longitudinal edge studies. Using a forest simulator, I designed and implemented a clear-cut on a forest stand replicating that of a *Populus*-dominated mixed-wood boreal forest. I then developed mathematical models fitted to the simulated data to describe the trends in the shade-intolerant tree populations over 70 years post-harvest. My objectives were:

(i) Develop mathematical models to explain how shade-intolerant tree populations respond to the creation of a clear-cut edge in a mixed-wood boreal forest dominated by *Populus* species. These models captured the changes in population over time and will range in complexity to reflect observations from the simulated data.

(ii) Assess the effectiveness of the constructed models in fitting the data and select the most suitable models based on their performance. Subsequently, I tested these chosen models to evaluate their reliability, robustness, and accuracy in making predictions.

As global fragmentation of landscapes continues to increase, understanding the effects of edges on ecosystems is becoming increasingly important. While there has been significant effort by edge researchers to better understand the effect of edges on varying ecosystems, characterizing vegetation responses to edge creation poses a unique challenge given the diverse nature of edge responses. As such, the construction of mathematical models that can be used to describe varying systems can provide an

accessible medium in which to test edge effects, but also to evaluate the long-term consequences of these effects. Furthermore, these models can provide insights into the underlying mechanisms that drive vegetation edge responses. Overall, mathematical models can provide us a means in which to further explore how edges influence forest ecosystems and assist in addressing missing longitudinal edge studies.

Chapter 2

The SORTIE-ND Forest Simulator

2.1 Introduction

The lack of longitudinal edge studies in combination with inconsistency in measured variable vegetation responses across studies poses a challenge to constructing and testing complex mathematical models rigorously. In the absence of empirical data, forest simulators are often used by researchers to better understand forest dynamics in changing environments (Moran et al., 2021). Coates et al. (2003) describe these simulators as capable of providing researchers a means to examine complex stand interactions, especially in the absence of relevant long-term field experiments. Forest simulators such as JABOWA (Botkin, 1993), FORSKA (Leemans & Prentice, 1989), ZELIG (Urban, 1990), PICUS (Lexer & Hönninger, 1998), FORMIX (Huth et al., 1998), ROPE (Shao & Shugart, 1995), and MOSAIC (Urban et al., 1999) were all developed to better understand and explore the interactions between forest stands and specific environmental conditions such as light, wind, and stand structure. Similar in concept, the SORTIE-ND forest simulator is an individual-based, spatially explicit forest successional model designed to investigate the interactions between individual

trees and the surrounding stand environment (Canham, n.d.). SORTIE-ND, as it is commonly known today, was adapted from the program SORTIE, which was in use from 1996 to 2004. SORTIE-ND provides all the capabilities of SORTIE, but with an additional emphasis on neighbourhood dynamics, hence the addition of "ND" to the original program name.

The capabilities of the SORTIE-ND program has led to its use in a variety of applications in forest management, biodiversity conservation, and climate change research (Canham, n.d.). The flexibility of the SORTIE-ND simulator allows it to be calibrated to simulate a wide range of diverse forest stands across the world (Ameztegui, Cabon, et al., 2017; Ameztegui, Paquette, et al., 2017; Canham & Murphy, 2017). A study conducted by Benson et al. (2022) involved a comparison of the SORTIE-ND model with other simulators. The findings of this study found that SORTIE-ND often outperformed other available models. They further elaborated on the attributes of the simulation, describing its individual-based implementation and how this property allows for investigations into fine-scale spatial concerns and localized processes. Furthermore, the simulator is spatially explicit enabling it to account for spatial dimensions including interactions between individual trees based on their proximity and size. This attribute allows the model to capture effects in both localized processes and the entire heterogeneous environment. Other favourable attributes investigated in this review included the allowance of multiple species, simplified processes (removing the requirements for technical complexity and difficult-to-measure physiological parameters), numerous optional modules, and the fact that it is a freely available and has a well-documented software package.

Before conducting simulated experiments, many studies using SORTIE-ND for data

collection validate the model by comparing its outputs to observed data. For instance, Moran et al. (2021) tested the simulator with 20 simulations using historical climate data and found that, in almost all cases, simulated mean growth and mortality fell within a 95% confidence interval of the observed values. Similar validation procedures were employed by Soubeyrand et al. (2023), where the model's performance in reproducing observed species assemblages was assessed, showing consistent results within a 95% confidence interval.

Coates et al. (2023) emphasize that the requirements and expectations of a forest simulator can influence its development, testing, and validation. SORTIE-ND, being a parametrized model, requires calibration with observed data for accurate predictions. Yet, excessive calibration can limit its capacity to address research questions. Combining parameterized SORTIE-ND models with experimentation or empirical sampling may offer a solution to this challenge.

2.2 Background

The Canham (n.d.) webpage (`http://www.sortie-nd.org/`) provides further information on the basic SORTIE-ND modelling concepts, which can be categorized as the state data, behaviours, simulation, and the parameter file. The state data defines the plot, the trees, and the grids. The plot is the geographical location where the stand simulation is occurring, the trees compose the individual trees occupying the plot, and the grids hold more specific data such as light levels and soil chemistry. The behaviours are the processes that occur to alter the state of the simulated stand. For SORTIE-ND, the behaviours often coincide with biological processes that are occurring within the stand. The simulation runs the behaviour and state data over a predetermined number of time-steps (each of length one year). At each time-step, a

sequence of behaviours is completed, thereby updating or changing the individual tree data and allowing for changes, such as growth, mortality, and recruitment, to occur within the stand. All the state data, behaviours, and simulation times are stored in a parameter file which allows users to easily run a variety of simulations of specific stand structures without the need to redefine the simulation.

The behaviours of SORTIE-ND are numerous and allow for detailed control over the simulation (Canham, n.d.). Simulation behaviours include state change, harvest and disturbance, management, light, growth, mortality, substrate, epiphytic establishment, mortality utility, snag dynamics, dispersal, seed predation, establishment, planting, and analysis. The state change behaviour informs model variables such as monthly and annual climate data. Harvest and disturbance behaviours allow the user to define disruptions in forest succession, including storm disturbances, forest harvesting regimes, and insect infestations. The management behaviour classifies trees based on their likelihood to die before the next harvest and their saw log potential. For trees in the SORTIE-ND model, light is a key resource. Light behaviours are implemented for individual trees at each time-step to calculate the amount of light each tree receives. The growth behaviour defines and determines the change in height and diameter of an individual tree by calculating dimension changes using related or independent growth equations. Mortality behaviours calculate tree death due to natural life cycle causes and stand competition. Mortality behaviours related to harvest and disturbance regimes are not included in this behaviour. Substrate behaviours track and determine substrate conditions at varying locations within the plot, which is especially important for seedling establishment. Epiphytic behaviour is additionally considered in the model, allowing epiphytes to spread and grow on individual trees

in the plot. Model behaviours such as mortality utility and snag dynamics allow the model to track the location of dead trees and remove decayed trees from the simulation. To ensure new growth is present in the model, the dispersal, seed predation, establishment, and planting behaviours determine how seedlings are spread and their survival rates, as well as intentional planting. Finally, the analysis behaviour prepares data for the final model output.

Randomness often observed in natural processes is also a consideration within the model (Canham, n.d.). Many defined behaviours in the SORTIE-ND simulation are determined stochastically. Model behaviours draw on probability distribution functions to make decisions during each time-step. For example, a tree's probability of mortality due to a wind storm and seedling spatial dispersion are behaviours calculated using probability distributions.

The simulation itself is intricate, using a set of state equations to describe behaviours (Canham, n.d.). These mathematical equations define the progression of the model at each time-step. The SORTIE-ND model structure can be broken down into various object types and relationships (Figure 2.1). The objects refer to various components of the models including the trees, plot, grids, behaviours, etc. The SORTIE-ND model structure also includes objects used to manage and implement the simulation including the simulation manager, sub-managers, and outputs. Objects are connected by either a control relationship or an interaction. Interactions act as communication between two objects in which there is an exchange of information. Control relationships act as an authoritative relationship whereby one object directs the behaviour of another. SORTIE-ND uses a C++ core representing all of the objects and relationships required to run a simulation. The user interacts with SORTIE-ND through

a Java interface. The Java interface is not fundamental to the overall function, but rather provides the user with the ability to interact with model input and output.

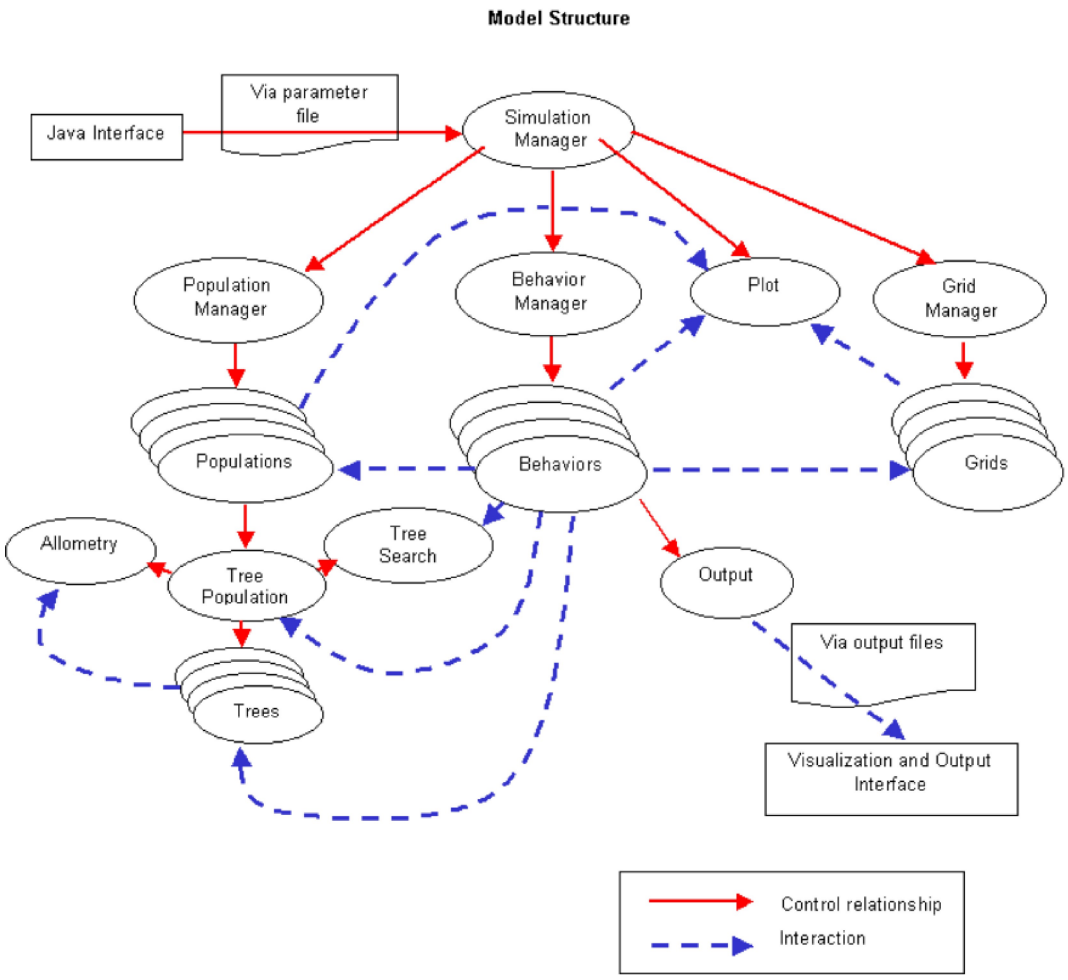

Figure 2.1: An illustration of the relationship between object types defined by the SORTIE-ND model. Reproduced from Canham (n.d.).

2.3 Methods

The parameter file used in my simulation, provided by Bose et al. (2015), simulated a trembling aspen (*Populus tremuloides* Michx)-dominated stand in eastern Canada. The parameter file describes 7 tree species including white cedar (WC), balsam fir (BF), mountain maple (MM), white spruce (WS), Jack pine (JP), trembling aspen (TA), and paper birch (PB). The 200 m by 200 m plot was initially populated with

each tree population (Table 2.1) and are randomly dispersed across the plot. The model was run for 200 time-steps (200 years), each time-step of length 1 year; no disturbances were introduced to the stand until time-step 100 to allow for sufficient growth. At time-step 100, a 40 m by 200 m clear-cut harvest was imposed on the western edge of the plot (Figure 2.2). The model was then run for the remaining 100 time-steps uninterrupted.

Table 2.1: Populations with trees of each species randomly dispersed across the SORTIE-ND plot.

Size Class	WC	BF	MM	WS	JP	TA	PB
5.0 - 7.0 cm	10.0	25.0	0.0	50.0	0.0	0.0	75.0
12.0 - 14.0 cm	0.0	0.0	0.0	0.0	0.0	50.0	0.0
14.0 - 16.0 cm	0.0	0.0	0.0	0.0	0.0	150.0	0.0
16.0 - 18.0 cm	0.0	0.0	0.0	0.0	0.0	100.0	0.0
18.0 - 20.0 cm	0.0	0.0	0.0	0.0	0.0	150.0	0.0
20.0 - 22.0 cm	0.0	0.0	0.0	0.0	0.0	125.0	0.0
22.0 - 24.0 cm	0.0	0.0	0.0	0.0	0.0	50.0	0.0
24.0 - 26.0 cm	0.0	0.0	0.0	0.0	0.0	150.0	0.0
26.0 - 28.0 cm	0.0	0.0	0.0	0.0	0.0	100.0	0.0
28.0 - 30.0 cm	0.0	0.0	0.0	0.0	0.0	25.0	0.0
30.0 - 32.0 cm	0.0	0.0	0.0	0.0	0.0	50.0	0.0
32.0 - 34.0 cm	0.0	0.0	0.0	0.0	0.0	50.0	0.0
34.0 - 36.0 cm	0.0	0.0	0.0	0.0	0.0	25.0	0.0

All data directly following the clear-cut were collected and stored from the simulation using the time-step tree-writer functionality. This function provides an output of

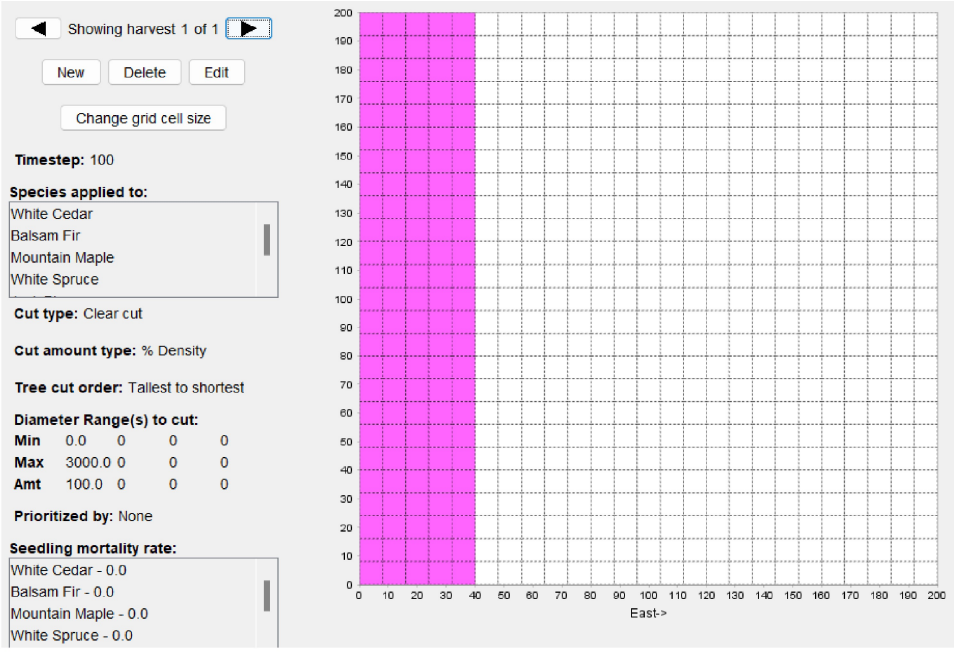

Figure 2.2: The 40 m by 200 m clear-cut harvest behaviour, represented by the pink shaded grids, that was implemented on the forest stand in the SORTIE-ND simulation at time-step 100.

a comprehensive text file detailing the condition of each individual tree in the plot at a specified time-step. Data provided in this text file include species type, tree mortality status, x and y coordinate locations in the plot, tree measurements (height, diameter, and crown radius), light availability, and how much growth had occurred. For further data analysis, the text files were converted to Excel files. These Excel files, one per time-step, were then collated as sheets within a master Excel file containing the entirety of the simulation run after the introduction of the clear-cut harvest behaviour.

Each Excel sheet was read into a Python script using the function *read_excel* from the Python Pandas library. The output provided by SORTIE-ND defines each tree type as a seedling, sapling, or adult. I categorized the population data into different life stages. Then, I separated dead and alive seedlings, saplings, and adults at a specified distance from the harvest site edge, storing them as separate arrays. Distances were categorized in 10 m increments by checking the x location provided for each individual

tree in reference to the edge of the clear-cut harvest. The distance arrays included trees in the ranges 0 m - 10 m, 10 m - 20 m, 20 m - 30 m, and so on, until 100 m into the interior forest. Additionally, I categorized the tree species populations as defined in the simulation as either shade-tolerant or shade-intolerant. Once these data were organized, the data for tree populations were also stored in arrays. Following the parsing procedures, the arrays stored within the Python script were categorized by the distance from the edge, the life stage, the dead code, and whether the species was shade-tolerant or shade-intolerant.

2.4 Results

From the simulation, I collected 63 usable time-step files following the clear-cut harvest that were then passed to Python for further processing. At various time-steps throughout the simulation, the model did not produce usable data. This unusable data were omitted from the data set. From the simulation results, it was clear that the shade-intolerant tree populations were more abundant from 0 m - 10 m from the edge of the harvest and had more extensive population changes after edge creation (Figure 2.3). From 0 m - 10 m from the edge, there is an observable spike in the shade-intolerant seedling population directly after edge creation.

However, the response of shade-tolerant species to edge creation was notably subdued. Unlike shade-intolerant species, there was no increase in the seedling population following edge creation (Figure 2.4). Moreover, the population of shade-tolerant tree species was significantly smaller than that of the shade-intolerant species, reinforcing the idea that the shade-tolerant species were not suitable candidates for informing edge model dynamics. As a result, after categorizing the data produced from the SORTIE-ND run, I decided to focus solely on the shade-intolerant tree populations

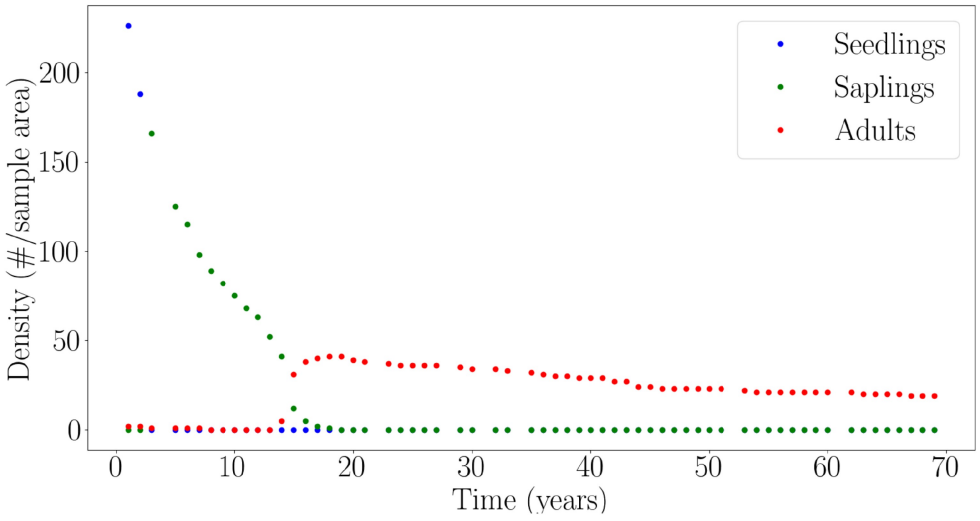

Figure 2.3: Shade-intolerant seedling, sapling, and adult populations from 0 m - 10 m from the edge of the harvest into the interior forest.

immediately after edge creation.

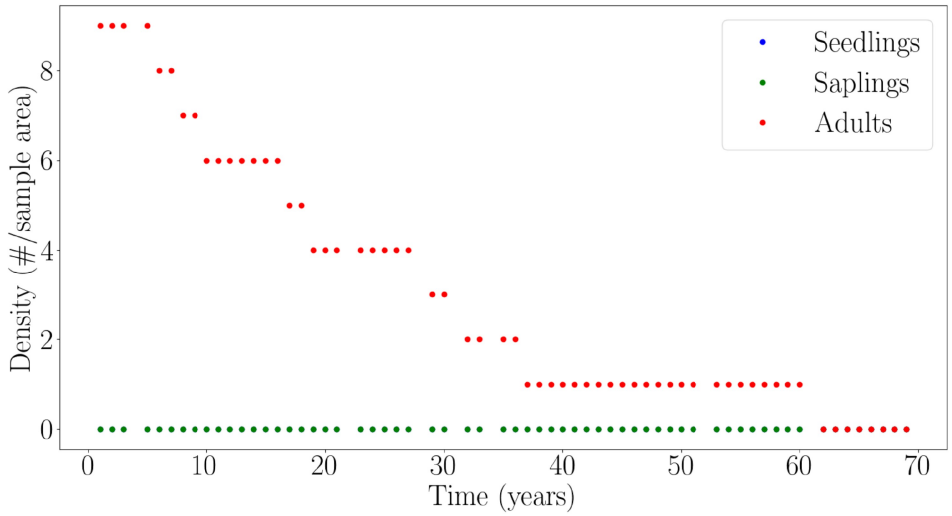

Figure 2.4: Shade-tolerant seedling, sapling, and adult populations from 0m - 10m from the edge of the harvest into the interior forest.

Chapter 3

Age-Structured Ordinary Differential Equation Models of Shade-Intolerant Tree Population Responses to Edge Creation

3.1 Introduction

Forest edges, also known as transition zones, are crucial landscape features as they modify the exchange of organisms, energy, and materials between adjacent habitat patches (Ries & Sisk, 2004). In the last three decades, Franklin et al. (2021) reported significant efforts have been devoted to understanding the global impact of edges on habitat conditions. The studies evaluated in this synthesis used various measured forest structure and composition response variables to assess environmental changes associated with edge creation. However, edge responses are system-specific and can vary given edge orientation, patch contrast, and temporal patterning (Ries & Sisk,

2004). As global fragmentation of forests increases, studying the influence of edges on diverse forest types poses limitations for empirical edge studies. In this regard, mathematical models offer an alternative approach to capture and describe these complex systems under different conditions, without requiring physical experimentation (Morozov, 2013).

Mathematical models are used in forest edge research to gain a deeper understanding of how edge dynamics impact the adjacent interior ecosystem (Ries & Sisk, 2004). These models offer the ability to describe intricate, non-linear responses observed empirically in the data (Ewers & Didham, 2006). Forest modelling, particularly in the context of edge dynamics, encompasses both stochastic and deterministic approaches (Menard et al., 2002). Vanclay (2006) defines deterministic models by their use of differential equations or Markov chains and their consideration of physical, biological, and climatic factors to define edge structure and composition. In contrast, they characterize stochastic models by their ability to accommodate the inherent unpredictability frequently encountered in ecological processes. Using both deterministic and stochastic processes, Vanclay (2006) describes agent-based spatially explicit succession models, such as SORTIE-ND, as capable of simulating complex forest scenarios under varying environmental stressors.

Generally, a model consists of two key components: model mechanics and model parameters (Read et al., 2020). Model mechanics describe the overall dynamics of a system, while model parameters enable fine-tuning to specific scenarios (Schroers, 2011; Read et al., 2020). By incorporating data from which the parameters may be estimated, models can be customized to accurately represent a system and yield predictions about its future state (Evans et al., 2013).

In this chapter, I investigate mathematical models for the representation of the SORTIE-ND simulated data, associated with shade-intolerant trees, that were discussed in Chapter 2. For this, I consider systems of age-structured ordinary differential equation (ODE) models. ODE models are used to describe the rate of change of an observed variable with respect to an independent variable, most often, time. ODE models can exhibit varying characteristics by incorporating either deterministic or stochastic processes, or a blend of both, depending on the specific problem. In this case, I define the ODE model using deterministic processes, where the model solutions are predictable given the initial conditions and governing equations Schroers (2011). This modelling approach captures distinct stages of tree growth (seedlings, saplings, and adults) and how tree populations are influenced by a clear-cut edge over time.

Here, I present a series of mathematical models constructed to describe the dynamics of a shade-intolerant tree population located at the edge of a clear-cut harvest. My objectives were to:

(i) Construct mathematical models capable of describing the dynamics of age-structured, shade-intolerant tree populations near a clear-cut forest edge. These models vary in parameter complexity to assess the necessary level of detail for describing the data, guided by trends observed in the simulated data from Chapter 2.

(ii) Within the model cohort, I will compare the models and identify the best models based on performance. Additionally, I conduct sensitivity analyses on these top-performing models to assess their robustness and enhance confidence in predictions.

(iii) Explore the capabilities of these models to perform at varying distances from the edge. As my main research goal was to mathematically describe how shade-

intolerant tree populations respond to edge influence, I was particularly interested in exploring this objective.

3.2 Methods

3.2.1 Model Development and Testing

Designing and validating age-structured ordinary differential equation (ODE) models entails a systematic process encompassing four key stages (Figure 3.1). First, ODE models undergo construction, involving the introduction of new parameters and coefficients to accurately represent observed behaviours in the data. Subsequently, model parameters and coefficients are optimized using a fitting procedure. Following this, models are compared within the cohort to identify the top performers. Lastly, the most promising models are subjected to sensitivity analyses, yielding additional insights into their reliability and robustness.

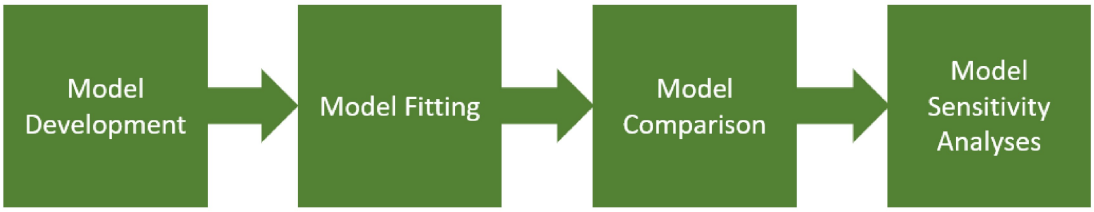

Figure 3.1: Description of the methodological process to construct and test the age-structured ODE models.

3.2.1.1 Model Development

To construct age-structured ODE models, I initially drew inspiration from the classic compartmental Susceptible, Infected, Recovered (SIR) model proposed by Kermack et al. (1997). This model describes a population where individuals are classified into three sub-populations given their disease status. I modified the model's structure to

accommodate an age-structured compartmental framework specifically designed for shade-intolerant tree populations located at the forest edge. In this modified model structure, trees are compartmentalized and transitioned between stages based on their current status as seedlings, saplings, or adult trees (Figure 3.2). In addition to modi-

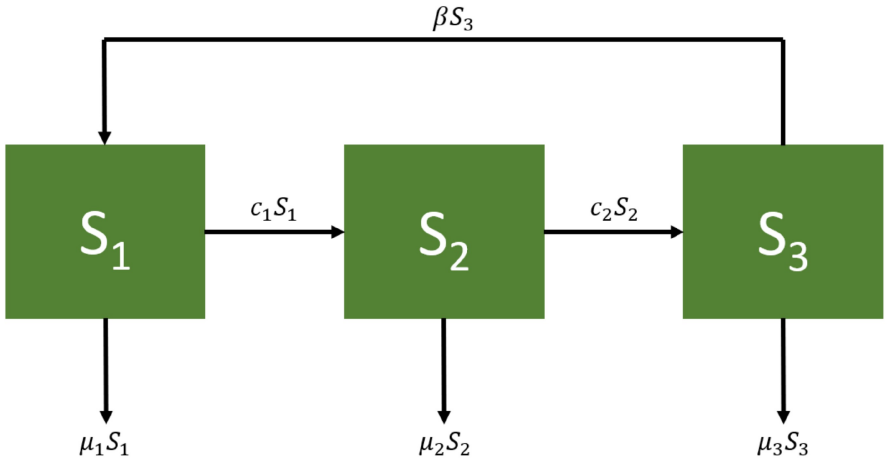

Figure 3.2: Vizualization of the adapted SIR model to the seedling (S_1), sapling (S_2), and adult (S_3) compartmental structure. Here, β represents the seedling establishment rate, c_1 and c_2 represent the seedling and sapling maturation rates, and μ_1, μ_2, and μ_3 represent the seedling, sapling, and adult mortality rates.

fying the compartmental structure, I also considered the parameters of the SIR model. These parameters govern population changes through birth, death, and recovery rates, as well as interactions between populations that allow susceptible individuals to become infected. I adopted a similar approach to define mortality, establishment, and maturation rates for shade-intolerant tree populations, thereby defining the movement of individuals within the age-structured compartments. To enhance the consistency between simulated data and model solution curves, I introduced systematic generalizations for certain parameters. These parameters were generalized to be time-dependent functions, utilizing unitless coefficients to enhance flexibility in the fitting process. By incorporating non-linear time-dependent parameter functions where suitable, I aimed

to better depict the population trends evident in the data. The resulting models formed a progression of nested structures, wherein each subsequent model retained the same underlying structural framework as its predecessors, but featured varying degrees of parameter complexity.

3.2.1.2 Model Fitting

Once conceptualized, models parameters were fitted to the data using a parameter optimization routine available within the Python scripting language (see Section 3.3.2). This iterative routine ensured an optimal fit for each model by continuously refining parameter values until no further improvements could be achieved. To maintain realistic parameter values, estimates for parameter values were bounded between 0 and ∞. The iterative adjustment process for model parameters continued until the difference between the ODE model solution curves and the simulated data could not be further minimized. To enhance the accuracy of this routine, a secondary Python function was developed to apply the routine a predefined number of times. During each iteration, the parameter values were compared with the previously stored values. If the current parameter values resulted in a superior fit compared to the previous best-fit values, the function updated the best performing parameter values and used them as the initial estimate for the next iteration of the routine.

3.2.1.3 Model Comparison

The fitted models were compared using the Akaike Information Criterion (AIC) (Akaike, 1998), a commonly used metric for comparing nested models (Wagenmakers & Farrell, 2004). The AIC considers the number of parameters present in the model, k, the number of data points, n, and the log of the likelihood, L (the likelihood of the model given the data) (Eq. 3.1). The likelihood, L, quantifies how well the model reproduces the

observed data, reflecting its accuracy in describing the underlying system's processes (Casella & Berger, 2002). However, calculating the likelihood can be challenging in many modelling cases (Rossi et al., 2020). As an alternative, the mean-squared error of the residuals (the difference observed between the data and the predicted model values), obtained by dividing the total sum of squared errors (SSE) by the total number of data points, n, can be used instead (Eq. 3.2) (Rossi et al., 2020). It is important to note that this approach assumes identical and independently sampled errors from a normal distribution for both the model and the data (Rossi et al., 2020).

$$AIC = -2 \cdot \ln(L) + 2 \cdot k \tag{3.1}$$

$$AIC = n \cdot \ln(SSE/n) + 2 \cdot k \tag{3.2}$$

I employed eq. 3.2 in order to calculate AIC values for my models.

AIC values were calculated for each model by comparing the residuals, i.e., the differences, between the solution curves and the simulated data points, and using these to calculate the SSE. Models were then compared using their calculated AIC score by calculating the difference between their score and the lowest AIC score of the model cohort. Since the magnitudes of the calculated model AIC values are not informative, the relative probabilities of the AIC scores were used to compare the models. For the ith model, the corresponding relative probability, $RelProb_i$, is given by the equation:

$$RelProb_i = e^{\frac{AIC_{min} - AIC_i}{2}}, \tag{3.3}$$

where AIC_{min} is the lowest AIC score of the model cohort and AIC_i is the AIC score of

the *ith* model. Models with relative probability scores less than 0.05 can be confidently rejected (Burnham & Anderson, 2003).

3.2.1.4 Sensitivity Analyses

A series of sensitivity analyses were conducted to assess the resilience of non-rejected models. These analyses explored the models' sensitivity to data noise, parameter variations, and structural changes. Overall, the investigations aimed to test the robustness and reliability of model predictions.

To assess the sensitivity of the models to noise added to the data set, I introduced noisy perturbations to the data. Specifically, for each classification of tree (seedling, sapling, and adult), noise was drawn from a normal distribution with a mean of 0. The variance was calculated based on the standard deviation between the model solution curves and the simulated data, separately for each population group. To create the noisy dataset, the data for each population group were perturbed by incorporating the population-specific noise realization. Each perturbed data was assessed to ensure the data remained non-negative. This process was repeated for every data point in the set. After generating the noisy data, model parameters were then refit to the perturbed data following the same parameter fitting procedure described earlier. Once the optimization process was complete, the new fitted parameters were saved. To ensure statistical robustness, I repeated this procedure 1000 times to obtain a sufficiently large sample size. The results of this test further inform confidence in the model predictions (Saltelli et al., 2008).

Critical parameters or coefficients are terms that have the most significant impact on model output. In order to determine which parameters or coefficients were critical, I employed the one-at-a-time (OAT) sensitivity test method (Razavi & Gupta, 2015).

The OAT method isolates each parameter or coefficient value, providing additional insights into critical parameters/coefficients, the reliability of model predictions, and any uncertainties present in the model (Saltelli et al., 2008). For the OAT method, all except one of the best-fit model parameter and coefficient values are held constant and the remaining parameter or coefficient is slightly perturbed by 5% increments relative to the parameter estimates, ranging from -25% to $+25\%$. Using the adjusted parameter or coefficient value, I generated new solution curves for the model. The sensitivity of a parameter or coefficient is determined based on the observed magnitude of difference between the baseline best-fit model solution curves and the perturbed model solution curves.

To evaluate model sensitivity under structural changes, I systematically modified the structure of a given ODE model in order to evaluate its performance under changing conditions. Model structure encompasses the arrangement, connectivity, and components that define the model's functional behaviour (Iooss & Lemaître, 2015). I examined how changes in parameter equation structure impacted model performance. In the simplest model, I considered all of the parameters to be constants. In my most complex models, some of the parameters were generalized to time-dependent expressions involving several coefficients (see equations 3.6a, 3.6b, 3.7a, and 3.7b). I systematically removed each parameter/coefficient that appeared in the parameter equations and re-ran the model predictions. This involved setting the removed parameters/coefficients to either 0 or 1. I removed isolated parameters or coefficients by setting their values to 0. For parameters or coefficients that had a multiplicative relationship with other parameters/coefficients, I removed them by setting their values to 1. This approach allowed me to isolate and assess the influence of specific parameters

or coefficients without affecting the others, especially when coupled with other parameters/coefficients. This analysis was performed for each parameter/coefficient in the model. The remaining model parameters/coefficients were then refit to the simulated data using the same fitting procedure outlined previously. To evaluate the model's response to the removal of a parameter/coefficient, I compared the AIC results of the simplified models to the original model's AIC results. This simplification process identifies model redundancies and unnecessary complexity (Iooss & Lemaître, 2015).

Finally, I tested how the models perform at varying distances from the edge of the clear-cut. By sorting the SORTIE-ND data in 10 m increments, I created data sets of seedling, sapling and adult shade-intolerant trees from 0 m - 10 m, 10 m - 20 m, 20 m - 30 m, etc. Using the same parameter fitting procedure, I refit the model parameters to the new subsets of data. Using the best fit parameters, I produced model solution curves and evaluated how well the model did at describing the data.

3.2.2 Solving Fitted ODE Models in Python

Model parameters and coefficients were fitted to the simulated SORTIE-ND data using two built-in functions available in the Python SciPy library (*SciPy*, n.d.). The *least_squares* function, found within the *optimize* subclass of the SciPy library, requires initial parameter/coefficient estimates along with a function that returns a calculated residual vector that represents the difference between the ODE model solution curve and the simulated data. The *least_squares* function uses the sum of squared errors of the residual vector to adjust the parameter/coefficient values until the residual vector is minimized. The function used to calculate the residual vector requires the use of an ODE solver to numerically calculate the solution to the ODE model for a given set of parameter/coefficient estimates. The ODE solver used, *odeint*, was accessed from the

SciPy.Integrate library. I now provide a brief overview of the algorithms employed by the ODE solver and the least squares optimization function.

3.2.2.1 Numerical Solutions to ODEs

The *odeint* function solves a system of ODEs using LSODA from the FORTRAN library odepack (*scipy.integrate.odeint — SciPy v1.9.3 Manual*, n.d.). LSODA is a further advancement of the FORTRAN subroutine package, LSODE, the Livermore Solver for Ordinary Differential Equations (Radhakrishnan & Hindmarsh, 1993). An ODE solver uses a numerical method in order to take a sequence of time-steps from the initial time to the final time. At the end of each time-step, an approximate solution point is completed. Solving a system of ODEs efficiently and accurately depends on the initial identification the stiffness of the ODE (Petzold, 1983). Stiffness can be generally characterized by rapid changes in the ODE solution, requiring small time-steps to ensure accuracy (Hindmarsh, 1992; Stroud, 1974). If an ODE is not stiff, it is said to be nonstiff. Nonstiff problems are often solved using explicit methods, such as Runge-Kutta and Adams methods (Hindmarsh, 1992). Stiff ODEs however, require a more nuanced solution approach as standard explicit methods applied to stiff problems lead to large computation times and possibly a loss in accuracy (Shampine & Gear, 1976). The reason for the extensive increase in computation time is due to the excessively small steps an explicit method has to take to solve a stiff ODE (Radhakrishnan & Hindmarsh, 1993). For stiff ODES, the LSODE solver uses a family of backward differentiation formulas (BDF) which can solve stiff problems without having to take very small time-steps (Gear, 1971). The LSODE package also includes a family of implicit Adams methods, which are useful for solving nonstiff problems (Radhakrishnan & Hindmarsh, 1993). Conveniently, the LSODA variant of LSODE

switches automatically between Adams and BDF methods using a stiffness detection algorithm developed by Petzold (1983) (Hindmarsh, 1992). This allows for optimal solution times for problems that change their stiffness over the time domain (Hindmarsh, 1992).

Assume that the ODE system to be solved has the general form, $\frac{d}{dt}\vec{Y}(t) = f(t, Y(t))$, with initial conditions, $\vec{Y}(t_0) = \vec{Y}_0$. The methods in the LSODE package generate approximate solutions, $\vec{Y}_n$, to the ODEs at discrete time points t_n, $(n = 1, 2, ...)$; hence $\vec{Y}_n \approx \vec{Y}(t_n)$ (Radhakrishnan & Hindmarsh, 1993). The solutions are approximated for each time point by using previous approximate solutions, $\vec{Y}_{n-j}$, that have already been computed for t_{n-j}, $j = (1, 2, ...)$ and previous function evaluations $\vec{f}_{n-j} = \vec{f}(t_{n-j}, \vec{Y}_{n-j})$, $(j = 1, 2, ...)$ (Radhakrishnan & Hindmarsh, 1993). The solutions are advanced at each time point t_n, using methods (called multistep methods) having the general form,

$$\vec{Y}_n = \sum_{j=1}^{K_1} \alpha_j \vec{Y}_{n-j} - h_n \sum_{j=0}^{K_2} \beta_j \vec{f}_{n-j} \tag{3.4}$$

where the coefficients α_j and β_j and the integers K_1 and K_2 are defined to give either an Adams method or a BDF. When $\beta_j \neq 0$, the multistep method is said to be implicit. This means that the formula computing $\vec{Y}_n$ uses the unknown value $\vec{f}_n = \vec{f}(t_n, \vec{Y}_n)$. In this case, a special numerical algorithm (e.g., Newtons method) must be used to compute the $\vec{Y}_n$ value.

3.2.2.2 Parameter and Coefficient Optimization

The *least_squares* function uses the Levenberg-Marquardt algorithm which employs both the Gauss-Newton method and the Levenberg method (Ranganathan, 2004).

The algorithm begins by using the Gauss-Newton method to solve the nonlinear least squares optimization problem (Levenberg, 1944). However, the Gauss-Newton method can be ill-suited for certain fitting applications, producing non-optimal parameter/coefficient fittings (Lourakis, 2005). In these cases, the algorithm will switch to the Levenberg method, which is an optimization method that deals with these specific fitting challenges (Levenberg, 1944).

Once parameter/coefficient values are estimated, the algorithm evaluates the magnitude of change between the previous estimates and the new estimates (Yuan, 1999). The algorithm uses the Trust Region Reflective method to control the size of the adjustments in the parameter/coefficient values during the optimization process (*Optimization and root finding (scipy.optimize) — SciPy v1.8.0 Manual*, n.d.). The algorithm employs a control on the size of the change in the parameter/coefficient values called a trust region (Branch et al., 1999). If the changes in the parameter/coefficient values fall inside the trust region, the changes are accepted and the algorithm moves to the next step in the process (Yuan, 1999). However, if some of the changes fall outside the trust region, the changes are rejected and the computation is adapted to reduce the parameter/coefficient adjustment size (Branch et al., 1999).

3.3 ODE Model Results: Development and Testing

3.3.1 Model Development

Model 1 retains the same framework as the original SIR model described earlier, except for the renaming of compartments to seedling (S_1), sapling (S_2), and adult (S_3) (Figure 3.2). The parameters of Model 1, assumed to be constant for this model, encompass the processes governing the establishment of shade-intolerant trees

as seedlings, their maturation into saplings and then adults, and their mortality (Table 3.1). Model 1 is described as follows:

$$\frac{dS_1}{dt} = \beta S_3 - c_1 S_1 - \mu_1 S_1, \tag{3.5a}$$

$$\frac{dS_2}{dt} = c_1 S_1 - c_2 S_2 - \mu_2 S_2, \tag{3.5b}$$

$$\frac{dS_3}{dt} = c_2 S_2 - \mu_3 S_3. \tag{3.5c}$$

Table 3.1: parameter definitions and units for Model 1.

Parameter	Definition	Units
β	Seedling establishment rate	$(Seedlings/Adults)/year$
c_1	Seedling maturation rate	$(Saplings/Seedlings)/year$
μ_1	Seedling mortality rate	$year^{-1}$
c_2	Sapling maturation rate	$(Adults/Saplings)/year$
μ_2	Sapling mortality rate	$year^{-1}$
μ_3	Adult mortality rate	$year^{-1}$

Using the SORTIE-ND simulated population data and the fitting procedure outlined in Section 3.2.1, I fit the parameters of Model 1 to the data (Figure 3.3). The analysis of the fitted results revealed distinct patterns in the data that were not adequately captured by the current structure of Model 1.

Upon evaluating the simulated data, I noticed a pronounced decline in the population of seedlings and saplings, particularly during the initial time periods. This decline in seedlings can be observed from time 1 to roughly time 6, while for saplings, it is

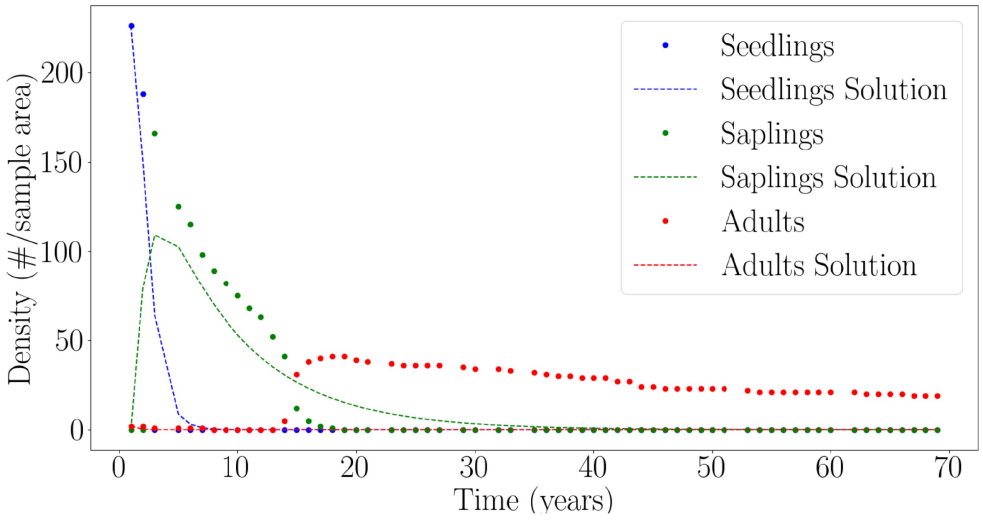

Figure 3.3: Solution curves of Model 1 solved using the best-fit parameters obtained via the curve-fitting procedures described in 3.2.1. The plot depicts the seedling, sapling, and adult model solutions at time t. Individual data points represent the seedling, sapling, and adult populations at time t from the SORTIE-ND simulated data set.

noticeable from time 3 to approximately time 10. Consequently, it became evident that the mortality rate for younger seedlings and saplings was notably higher compared to their more mature counterparts (Figure 3.3). To address this, I introduced new time-dependent mortality parameters, expressed as a negative exponential function plus a constant term commonly found in survivorship curves (Kimmins, 2003). In this context, an exponential function has the functionality to characterize the accelerated decline observed in the seedling and sapling population during the early stages of the simulation. It also effectively captures the subsequent, more gradual decline in population. The time-dependent mortality rates, μ_1 and μ_2, are defined as follows:

$$\mu_1 = f \cdot e^{-g \cdot t} + h, \tag{3.6a}$$

$$\mu_2 = i \cdot e^{-j \cdot t} + k. \tag{3.6b}$$

Here, f, g, h, i, j, and k represent unitless coefficients that provide flexibility for the representation of the mortality parameters, μ_1 and μ_2, and t denotes time. These generalized mortality parameters effectively capture the varying magnitude of population mortality, particularly noticeable in the seedling and sapling populations. Furthermore, the expressions for μ_1 and μ_2 in (3.6a) and (3.6b) allow the higher mortality in the younger seedling and sapling populations to diminish with time (Figure 3.4).

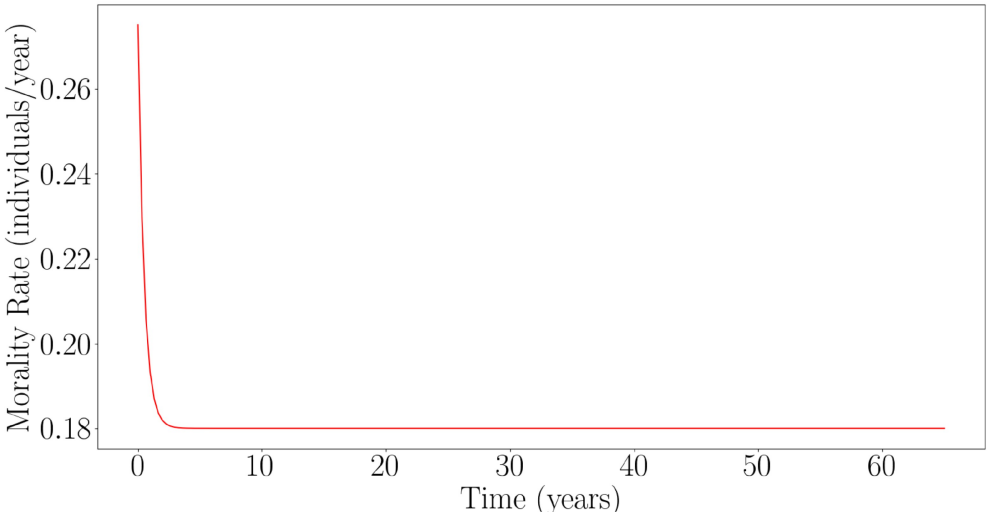

Figure 3.4: A general visualization of the trend of equations 3.6a and 3.6b. This plot gives a general depiction of how the mortality rate term, μ, changes over time.

For the maturation rates of seedlings and saplings, I observed from the SORTIE-ND data at approximately time 3, a significant number of seedlings transitioned into saplings. A similar trend was noticed for saplings transitioning into adults at roughly time 15. To capture this trend, I altered the maturation parameters. I employed generalized time-dependent sigmoidal functions for the maturation rates, c_1 and c_2, of the seedling and sapling populations. The properties of a sigmoidal function allows the maturation rate to quickly increase at the average time of maturation as observed in the data. Following this increase, the function will then level off. This general form

of this function is expressed in the following equations:

$$c_1 = \frac{\alpha}{1 + e^{-\gamma(t - t_{c_1})}} + \delta, \tag{3.7a}$$

$$c_2 = \frac{\sigma}{1 + e^{-\psi(t - t_{c_2})}} + \zeta. \tag{3.7b}$$

Here, α, γ, δ, σ, ψ, and ζ are arbitrary unitless coefficients, and t_{c_1} and t_{c_2} are coefficients representing the average maturation time for seedlings and saplings, respectively. By utilizing these generalized maturation rates, I was able to generalize the model to facilitate a substantial increase in the rate of maturation around the average maturation time. This enabled a substantial transfer of seedlings to the sapling compartment and saplings to the adult compartment consistent with what can be observed in the SORTIE-ND data (Figure 3.5).

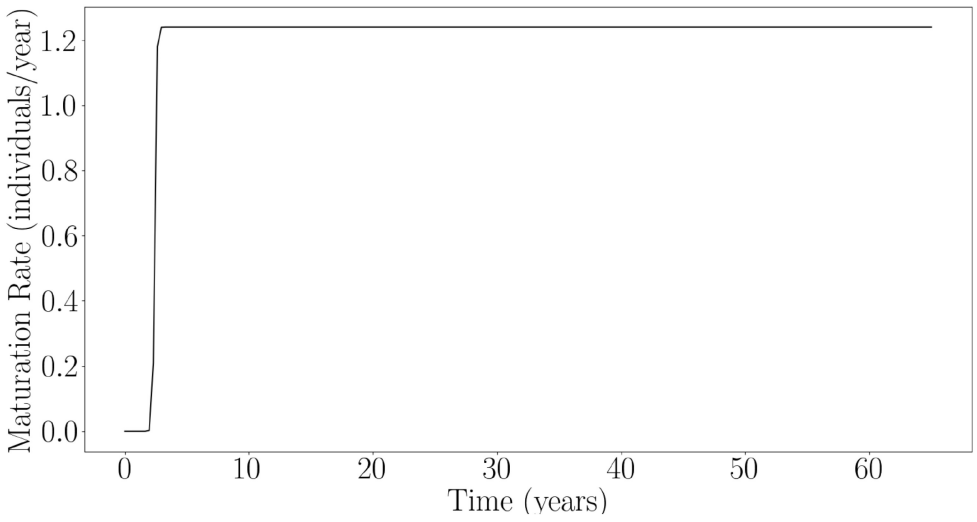

Figure 3.5: A general visualization of the trend of the equations 3.7a and 3.7b. This plot gives a general depiction of how the maturation terms, c, changes over time.

Based on these generalized parameters, I developed seven additional ODE models (Table 3.2). As each model is a more complex modification of Model 1, these are

considered to be nested models. Using these eight models, I explored how changes to the parameters altered the fitted results.

Table 3.2: Models and their associated updated parameters.

Model	Updated Terms
1	-
2	μ_1
3	c_1
4	μ_1, c_1
5	c_1, c_2
6	μ_1, μ_2, c_1
7	μ_1, c_1, c_2
8	μ_1, μ_2, c_1, c_2

3.3.2 Model Fitting Results

Model 1 served as my initial foundation for developing all other models. However, I observed that Model 1 did not accurately fit the observed data (Figure 3.6 A). While this model approximately captured the trend of the seedling and sapling populations, it deviated from the observed data after approximately 20 years. Additionally, the adult solution curve suggested no change in the adult population throughout the simulation, which contradicts the observed data.

Model 2 produced nearly identical fitting results to that of Model 1 (Figure 3.6 B). Recall, Model 2 included the introduction of the updated mortality term for the seedling population (Table 3.2). Model 2 solution curves approximately described the population trends; however, these still do not agree very well with the data. Similar to Model 1, Model 2 suggested no change in the adult population for the duration of the simulation, which did not accurately reflect the observed trends in the data. The results from this model suggested that the addition of the time-dependent mortality parameter for the seedling class alone was not sufficient to accurately describe the trends in the data.

Model 3 improved upon Model 1 by employing the updated seedling maturation rate (Table 3.2). However, the solution curves from Model 3 did a poor job of capturing all of the trends observed in the data across all populations (Figure 3.6 C). The solution curves suggested that the seedling population quickly decayed to 0 following the initial time period. Similarly, the adult solution curve showed no change within the adult population for the duration of the simulation. The sapling solution curve depicted an initial increase in the population following the decline of the seedling population. However, this solution curve fails to replicate the correct magnitude in which

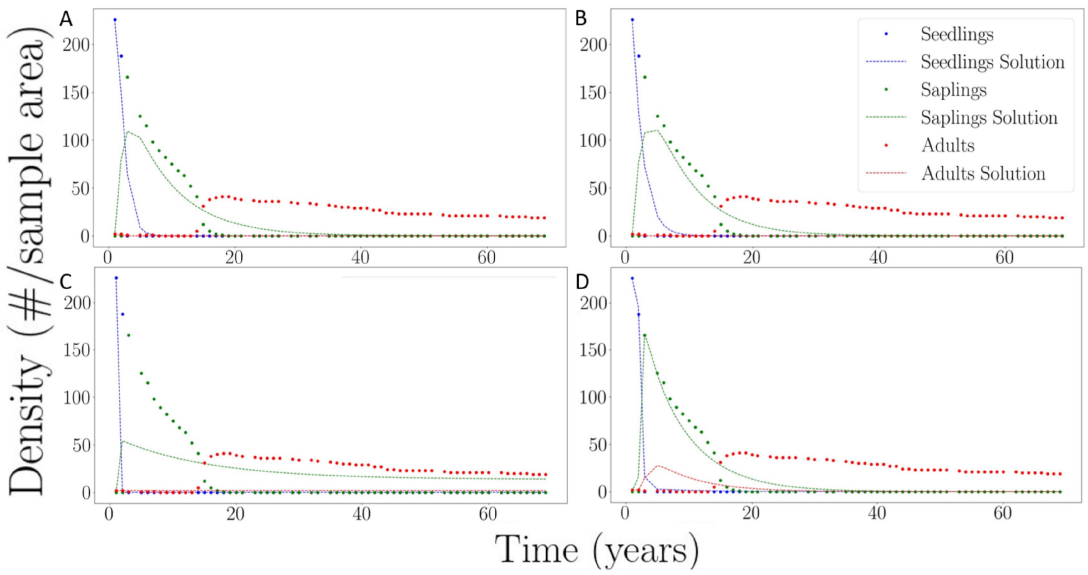

Figure 3.6: Solution curves obtained following parameter/coefficient fitting procedures for Models 1 - 4 (A-D). The plots depict the SORTIE-ND data and the fitted model solution curves for the changes in the seedling, sapling, and adult populations over time.

this change is observed in the data. Additionally, following the sapling population increase, the sapling solution curve appeared to approach a non-zero population value, contradicting the trends observed in the data. The results of the fitting indicate that the inclusion of the time-dependent seedling maturation rate not only fell short in accurately describing the data, but also led to a notably inferior fit compared to Models 1 and 2.

Model 4 included the addition of both time-dependent seedling mortality and maturation rates (Table 3.2). From the results of the fittings, it is clear that Model 4 produced reasonably accurate fitting results for the seedling population (Figure 3.6 D). Model 4 also did an adequate job in capturing the changes observed in the sapling population. More specifically, Model 4 was able to produce a sapling solution curve that reached the peak of the sapling population data, but also more accurately described the subsequent population decrease as seen in the data. Furthermore, Model

4 produced an adult solution curve that showed a marginal population change near the beginning of the simulation. Although the adult solution curve did not accurately describe the data, compared to other model adult solution curves, its better agreement with the data suggested that additional modifications to the models would potentially lead to improved fits. Given these results, I observed that while the alterations to the seedling mortality and maturation rates independently in Models 2 and 3 did not produce improved fits, applying both changes in Model 4 allowed this model to produce reasonably improved solutions.

To investigate how maturation rates influenced model behaviour, Model 5 employed both the updated seedling and sapling maturation terms (Table 3.2). From the results for Model 5, I observed that the adult solution curve did not remain at 0 for the entirety of the simulation (Figure 3.7 A). Moreover, compared to the previous models, this adult solution curve best reflects the observed trends in the adult population as depicted in the data. For the seedling and sapling populations, while the solution curves for the initial part of the simulation approximated the observed population trends in the data reasonably well, the model solution curves did not approach zero as the population declines. However, the improvement upon the adult solution curve indicated that further developments to the models would likely result in the desired outcome.

Model 6 included the introduction of the time-dependent seedling maturation and mortality rates as well as the time-dependent sapling mortality rate (Table 3.2). Unlike the previous models, Model 6 introduced changes to three of the original parameters from Model 1. The fitting results showed that Model 6 successfully captured the general trends observed in the data (Figure 3.7 B). While it was unable to precisely

fit the seedling and sapling population data, Model 6 did give solution curves that are able to represent the peaks observed in these populations as well as the decline of each population that follows. For the adult solution curve, I observed that the initial population increase was not accurately described by the solution curve. However, the solution curve did appear to reasonably approximate the long term population trend.

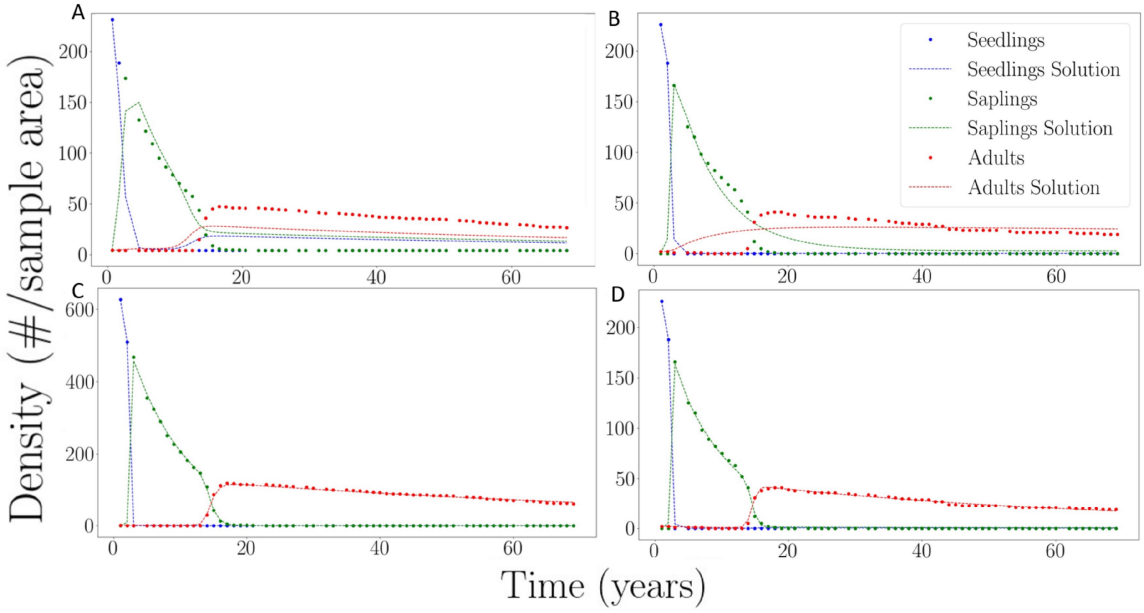

Figure 3.7: Fitting results for Models 5 - 8 (A-D). The plots depict the SORTIE-ND data and the fitted model solution curves for the changes in the seedling, sapling, and adult populations over time.

Model 7 included both time-dependent seedling and sapling maturation terms together with the time-dependent seedling mortality term (Table 3.2). Compared to the previous models, Model 7 appeared to produce the best overall fitting results (Figure 3.7 C). I observed that for all three populations, the model solution curves appeared to accurately describe the trends observed in the data. Based on these findings, Model 7 demonstrated the highest level of promise in accurately describing the population dynamics as observed in the data.

Model 8 included both the time-dependent seedling and sapling maturation and

mortality rates (Table 3.2). Similar to Model 7, the results for Model 8 indicated that the inclusion of all four improved parameters greatly improved the accuracy with which the model is able to capture the trends in the data (Figure 3.7 D). Model 8 solution curves accurately fit all three populations. The results for Model 8 suggested promising potential in accurately characterizing the overall population dynamics observed in the data.

3.3.3 Model Comparison Results

The number of parameters, SSE values, AIC scores (Eq. 3.2), and subsequent relative probabilities (Eq. 3.3) were calculated for all models (Table 3.3).

Table 3.3: Fit for Models 1 - 8 including the number of parameters, the SSE between the model solution curves and the observed data, the AIC score calculated using eq. 3.2, and the relative probability using eq. 3.3.

Model	Number of Parameters	SSE	AIC	Relative Probability
Model 1	6	61367.33	1090.59	3.47×10^{-225}
Model 2	8	62412.34	1097.73	9.79×10^{-227}
Model 3	9	124656.32	1228.40	4.13×10^{-255}
Model 4	11	44675.90	1041.54	1.56×10^{-214}
Model 5	12	43967.35	1040.57	2.53×10^{-214}
Model 6	13	10192.20	770.67	1.03×10^{-155}
Model 7	14	217.29	56.92	1.00×10^{0}
Model 8	16	239.95	79.37	1.33×10^{-05}

From these results, the best model was Model 7. Model 7 had the lowest SSE and a lower AIC score than any other models (Table 3.3). However, it is worth noting that Model 8 also produced a relatively low AIC score when compared with the other models. While Models 7 and 8 produced almost identical fitting results and have a relatively similar model structures, the additional parameters in Model 8 are not justifiable. Based on this observation, I further explored Model 7 to better understand its behaviour under varying conditions. The best-fit parameter and coefficient values for Model 7 are given in Table 3.4.

Table 3.4: Model 7 best fit parameter values and the lower and upper limit of a 95% confidence intervals.

Parameter	Best Fit Value	Lower Limit	Upper Limit
β	6.2432×10^{-2}	6.2059×10^{-2}	1.6459×10^{-1}
α	1.2438×10^{1}	1.1406×10^{1}	1.7469×10^{1}
γ	1.4171×10^{1}	1.2831×10^{1}	1.5805×10^{1}
t_{c_1}	2.3995×10^{0}	2.3227×10^{0}	2.6230×10^{0}
δ	1.2099×10^{-4}	1.1473×10^{-4}	2.2245×10^{-4}
σ	2.0450×10^{0}	1.1772×10^{0}	2.0471×10^{0}
ψ	3.1834×10^{0}	2.7889×10^{0}	4.7524×10^{0}
t_{c_2}	1.4486×10^{1}	1.4061×10^{1}	1.4545×10^{1}
ζ	2.0159×10^{-7}	1.4031×10^{-7}	4.5451×10^{-3}
f	9.5007×10^{-2}	2.1285×10^{-2}	5.4051×10^{-1}
g	2.0037×10^{0}	1.8886×10^{0}	2.3058×10^{0}
h	1.8531×10^{-1}	1.5913×10^{-1}	1.9837×10^{-1}
μ_2	1.1423×10^{-1}	1.0924×10^{-1}	1.1784×10^{-1}
μ_3	7.5009×10^{-2}	7.0079×10^{-2}	1.7005×10^{-1}

3.3.4 Sensitivity Analysis Results

3.3.4.1 Sensitivity to Noise in the Data

The sensitivity analysis for Model 7 revealed that the parameters/coefficients present in the model exhibited varying degrees of sensitivity to noise in the data. I classified the parameters/coefficients as not sensitive, moderately sensitive, or sensitive given the trends observed in the spread of the estimates (Table 3.5).

Table 3.5: Sensitivity analysis results for parameter sensitivity to noise. Parameters are classified as not sensitive, moderately sensitive, or sensitive.

Sensitivity	Parameters
Not Sensitive	α, γ, ψ, f, g
Moderately Sensitive	t_{c_1}, t_{c_2}, h, σ, μ_2
Sensitive	β, δ, ζ, μ_3

The parameters/coefficients that produced the most uniform fitting results, with the majority of estimates in agreement with or close to agreement with the best-fit parameter values, were classified as not sensitive to noise in the data (Figure 3.8). A number of parameters/coefficients showed spread in the estimates with a frequency distribution that exhibited clear distribution trends around the best-fit parameter values (Figure 3.9). These parameters/coefficients were classified as moderately sensitive to noise in the data. The remainder of parameters/coefficients produced a substantial spread in their frequency distributions (Figure 3.10). As such, these parameters/coefficients were classified as sensitive to noise in the data.

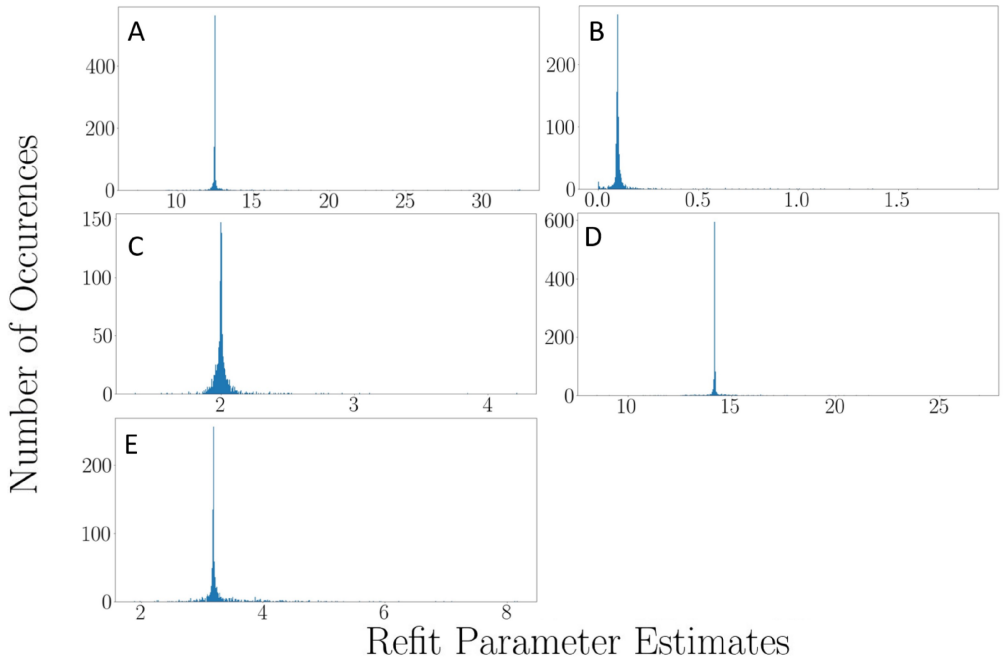

Figure 3.8: Frequency of parameter estimates produced for not sensitive parameter values α (A), f (B), g (C), γ (D), and ψ (E).

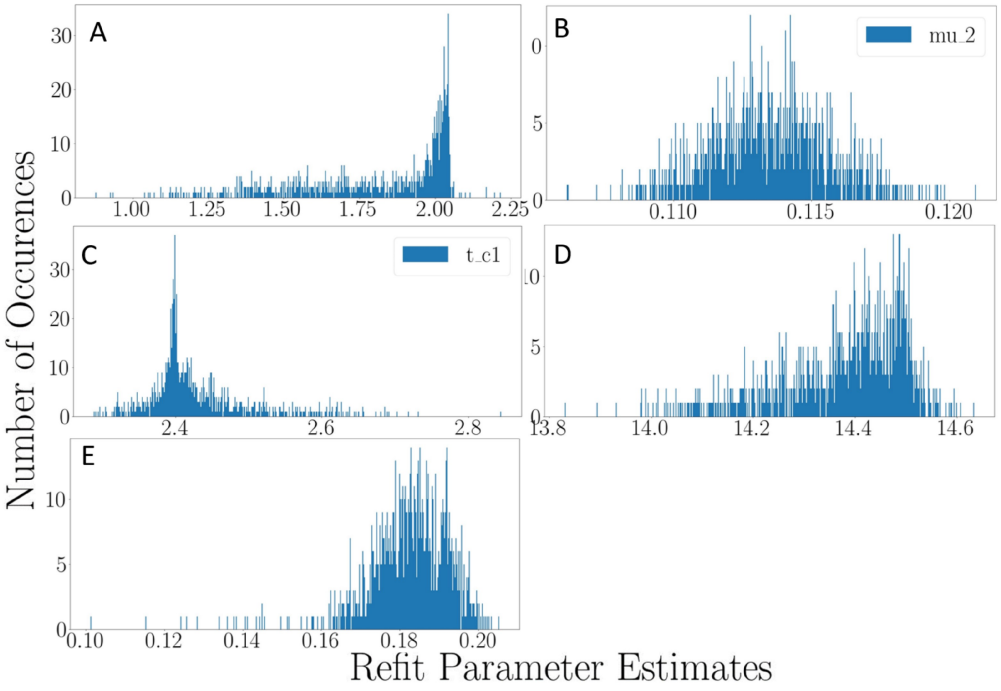

Figure 3.9: Frequency of parameter estimates produced for moderately sensitive parameter values σ (A), μ_2 (B), t_{c_1} (C), t_{c_2} (D), and h (E).

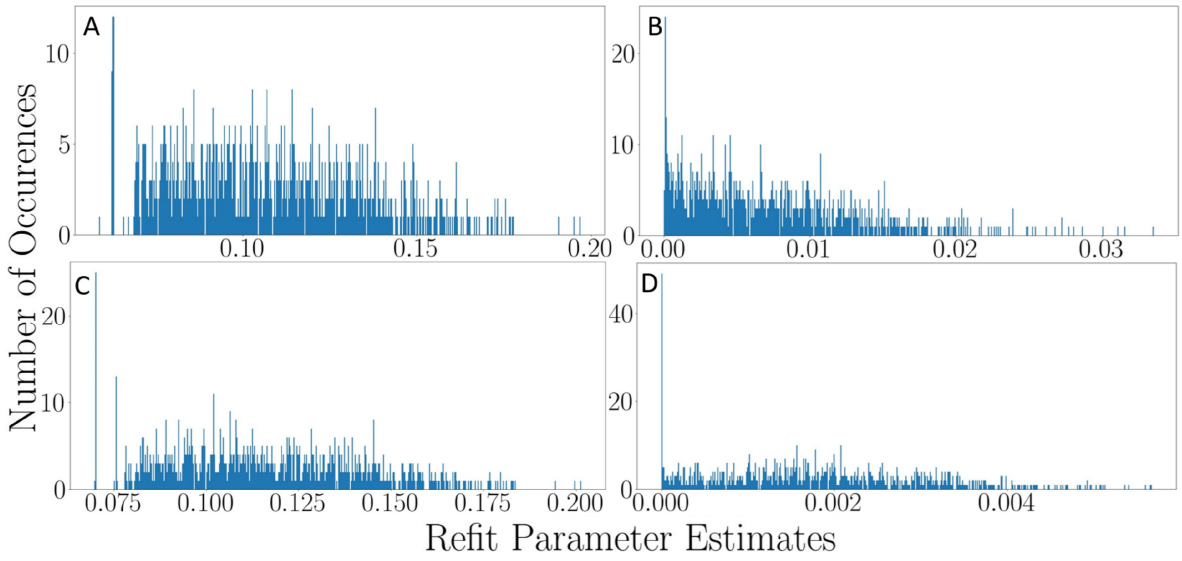

Figure 3.10: Frequency of parameter estimates produced for sensitive parameter values β (A), δ (B), μ_3 (C), and ζ (D).

3.3.4.2 OAT Sensitivity Analysis

Table 3.6: Model 7 sensitivity to noise in parameter/coefficient values results for each model compartment.

Parameter	Seedling	Sapling	Adult
β	Not Sensitive	Not Sensitive	Sensitive
α	Not Sensitive	Not Sensitive	Not Sensitive
γ	Not Sensitive	Not Sensitive	Not Sensitive
t_{c_1}	Sensitive	Sensitive	Sensitive
δ	Not Sensitive	Not Sensitive	Not Sensitive
σ	Not Sensitive	Not Sensitive	Sensitive
ψ	Not Sensitive	Not Sensitive	Not Sensitive
t_{c_2}	Not Sensitive	Sensitive	Sensitive
ζ	Not Sensitive	Not Sensitive	Not Sensitive
f	Not Sensitive	Not Sensitive	Not Sensitive
g	Not Sensitive	Not Sensitive	Not Sensitive
h	Not Sensitive	Not Sensitive	Sensitive
μ_2	Not Sensitive	Sensitive	Sensitive
μ_3	Not Sensitive	Not Sensitive	Sensitive

For each parameter/coefficient in Model 7, the OAT sensitivity test was implemented to evaluate how model solutions responded to slight perturbations in best-fit values (Table 3.6). Non-sensitive responses showed little to no deviations from the solutions curves produced using the best-fit values (see Appendix B). From this experiment, it was observed that changes made to coefficient value t_{c_1} influenced all three population solution curves (Figure 3.16). For the other parameters/coefficients,

I observed that varying specific values would only influence one or two populations. For the adult solution curve, model output was influenced by parameters/coefficients σ (Figure 3.11), β (Figure 3.12), h (Figure 3.13), μ_2 (Figure 3.14 B), μ_3 (Figure 3.15), t_{c_1} (Figure 3.16 C), and t_{c_2} (Figure 3.17 B). For the sapling solution curve, changes occurred when coefficients t_{c_1} (Figure 3.16 B) and t_{c_2} (Figure 3.17 A) were altered. The seedling model solution was only influenced by changes to the coefficient t_{c_1} (Figure 3.16 A).

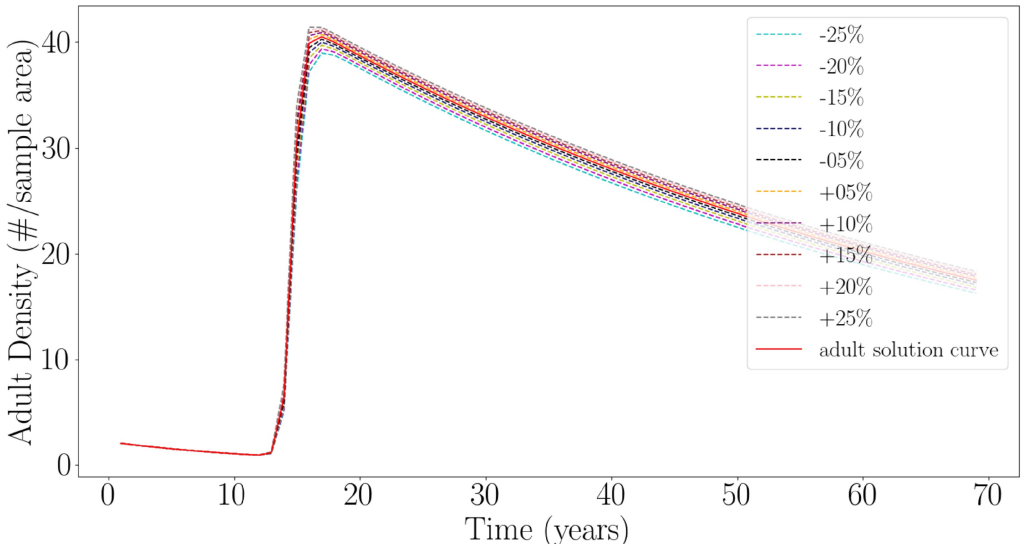

Figure 3.11: σ sensitivity results for adult tree populations over time; comparison of the adult model solution curve and subsequent solution curves after perturbing the coefficient σ.

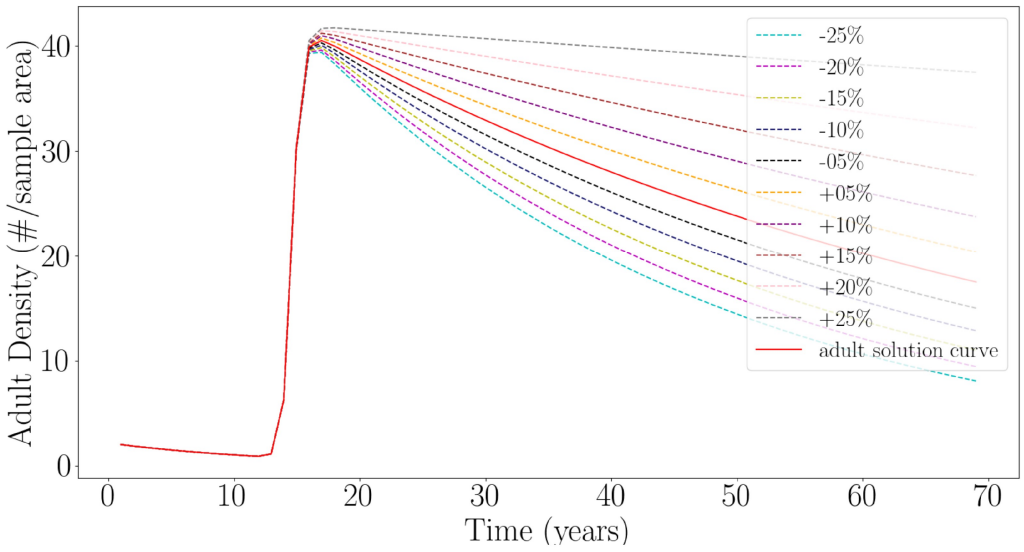

Figure 3.12: β sensitivity results for adult tree populations over time; comparison of the adult model solution curve and subsequent solution curves after perturbing the parameter β.

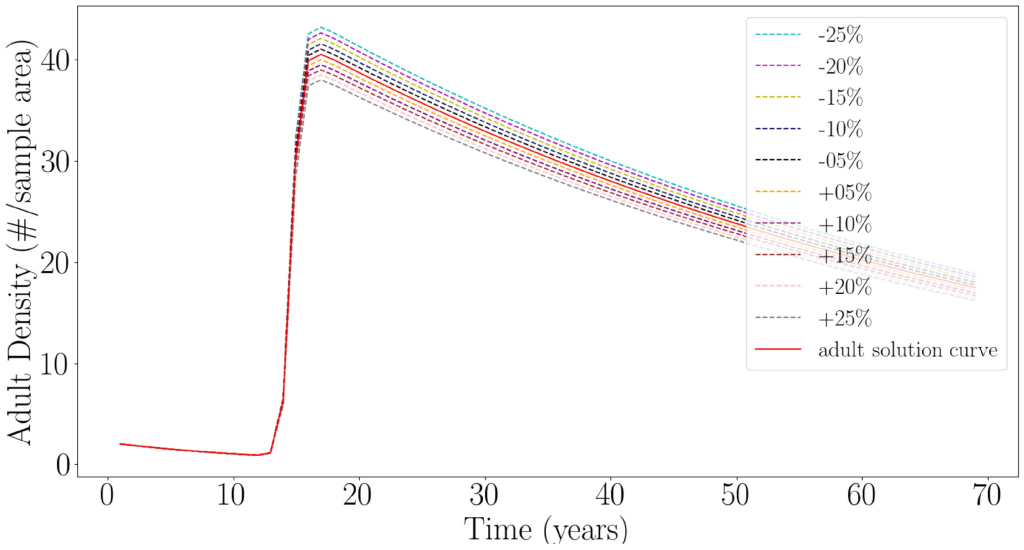

Figure 3.13: h sensitivity results for adult tree populations over time; comparison of the adult model solution curve and subsequent solution curves after perturbing the coefficient h.

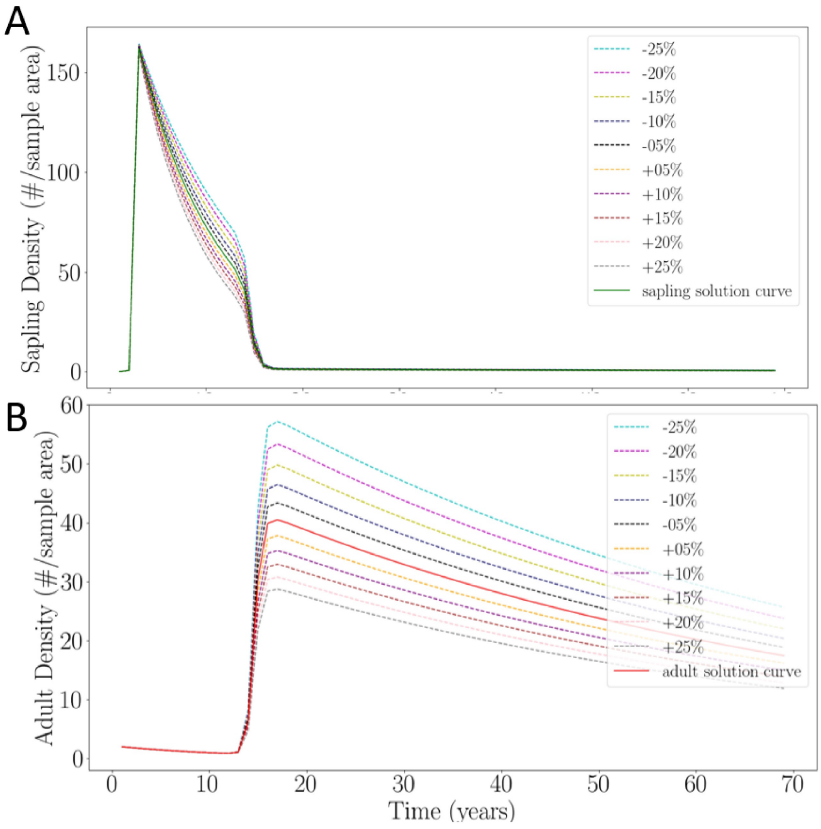

Figure 3.14: μ_2 parameter sensitivity results for the sapling populations (A) and the adult populations (B) over time; comparison of the sapling and adult model solution curves and subsequent solution curves after perturbing the parameter μ_2.

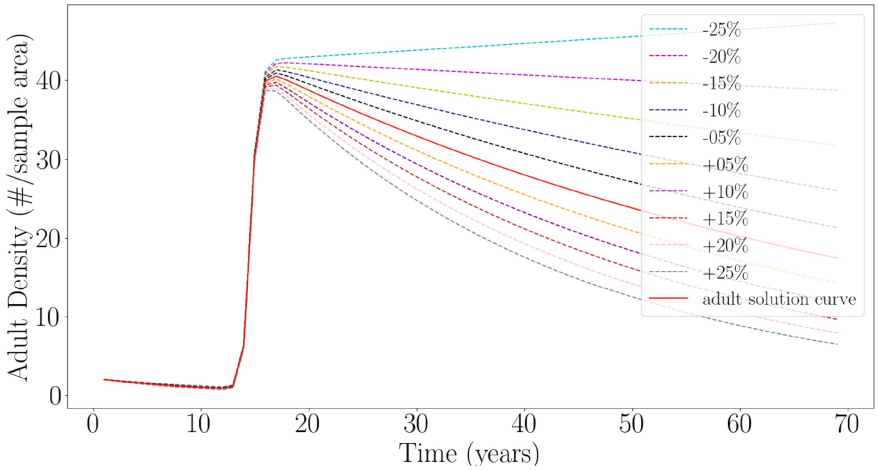

Figure 3.15: μ_3 parameter sensitivity results for adult tree populations over time; comparison of the adult model solution curve and subsequent solution curves after perturbing the parameter μ_3.

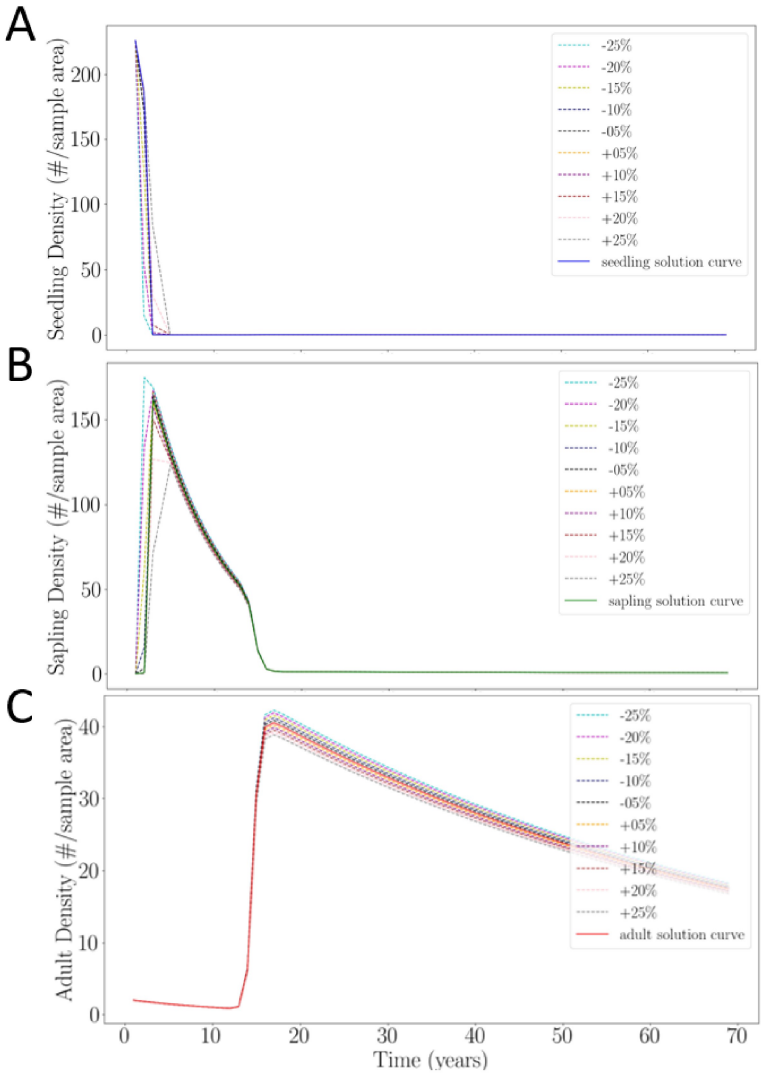

Figure 3.16: t_{c_1} sensitivity results for seedling populations (A), sapling populations (B), and adult populations (C) over time; comparison of the seedling, sapling, and adult model solution curves and subsequent solution curves after perturbing the parameter t_{c_1}.

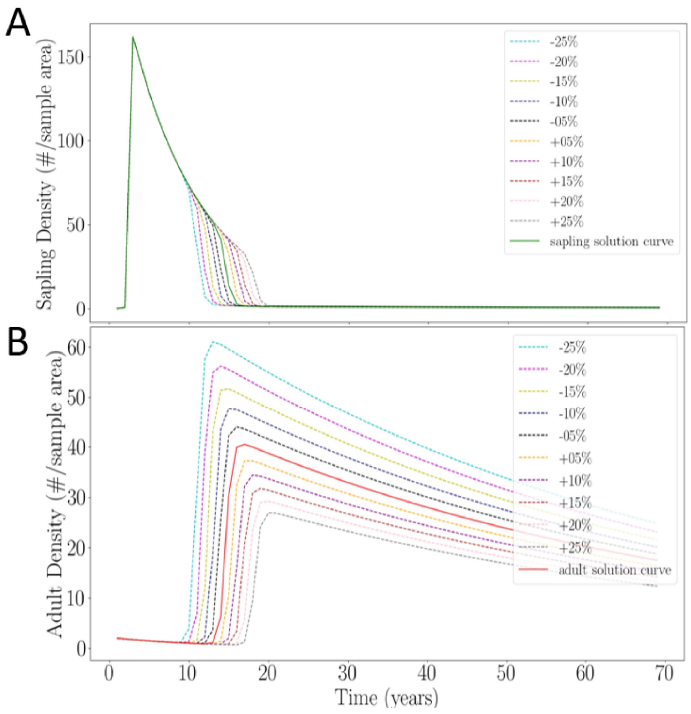

Figure 3.17: t_{c_2} sensitivity results for sapling populations (A) and adult populations (B) over time; comparison of the sapling and adult populations and subsequent solution curves after perturbing the parameter t_{c_2}.

3.3.4.3 Sensitivity to Model Structure

The results of the sensitivity to model structure test identified several parameters and coefficients as redundant to the structure of Model 7 (Table 3.7).

Table 3.7: Model 7 structure test results including the SSE and newly calculated AIC score. Parameters/coefficients were individually replaced in the model structure. Once replaced, the remaining model parameter/coefficients values were refit to the data. The replacement value in the right-most column indicates what value each parameter/coefficient was replaced with.

Removed Parameter/Coefficient	SSE	AIC	Replacement Value
β	194.48	34.29	0
δ	246.03	78.03	0
ζ	210.84	49.31	0
t_{c_1}	2077.09	903.15	0
t_{c_2}	43734.33	1041.59	0
α	7175.25	705.39	1
σ	219.59	56.88	1
γ	10827.73	781.93	1
ψ	570.04	234.31	1
f	276.29	99.60	1
g	220.19	57.38	1
h	303.53	117.09	0
μ_2	35938.52	465.82	0
μ_3	9523.16	1005.07	0

From these results, it can be seen that replacing the model parameters and coefficients, β, ζ, σ, and g (Figure 3.18 A-D), produced fitting results with SSE and AIC

scores that would not be rejected. Recall that the SSE and AIC score for the original Model 7 were 217.29 and 56.92, respectively (Table 3.3). This is a good indication that these four model parameters and coefficients may be redundant.

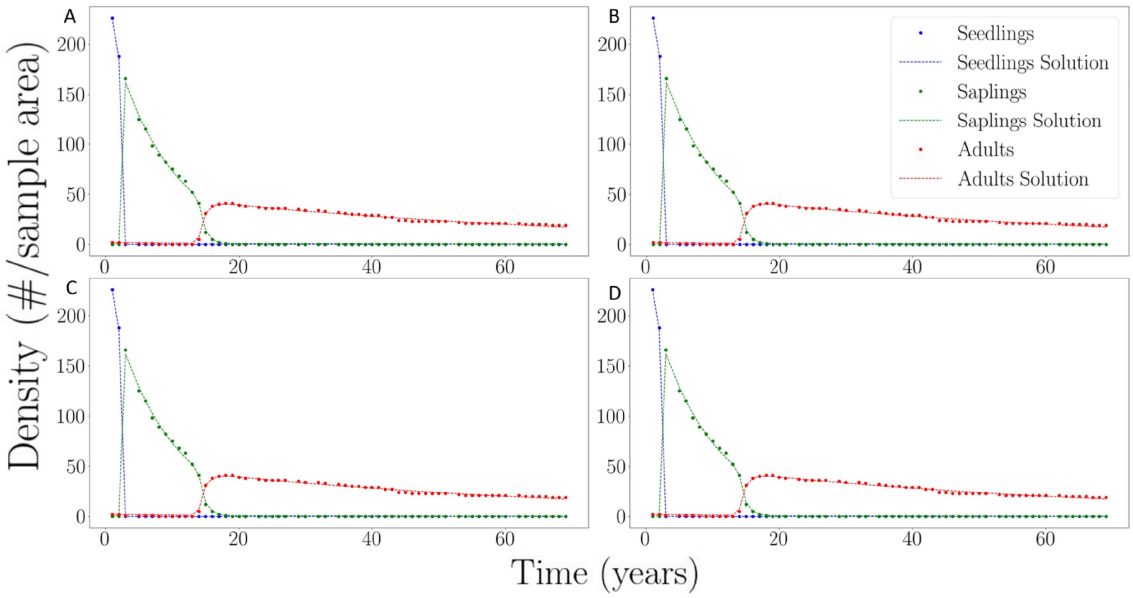

Figure 3.18: Model 7 solution curves of tree populations size over time resulting from the replacement of the parameters β (A), ζ (B), σ (C), and g (D).

Removal of subsets of each of the four identified parameter and coefficient values identified possible parameter/coefficient redundancies present in Model 7 (Table 3.8).

Replacements of combinations of the four identified parameter/coefficient values also produced good fitting results compared to that of Model 7. These included replacing ζ, σ, and g (Figure 3.19 A), β and ζ (Figure 3.19 B), β and σ (Figure 3.19 C), β and g (Figure 3.19 D), ζ and σ (Figure 3.19 E), and σ and g (Figure 3.19 F). Removing three or more parameters mostly produced poor results. It is notable, however, that while the coefficients ζ, σ, and g were not specifically assigned to any fundamental biological process, β is defined as the seedling establishment rate.

Table 3.8: Results of the replacement of subsets of the identified redundant parameters including the newly calculated SSE and AIC scores are shown here. Recall that the SSE and AIC scores for the original Model 7 are 217.29 and 56.92, respectively.

Parameter/Coefficients	SSE	AIC	Figure Reference
β, ζ, σ, g	23852.58	922.83	B.16 A
β, ζ, σ	22668.06	915.35	B.16 B
β, ζ, g	249.55	76.66	B.16 C
ζ, σ, g	192.39	28.25	3.19 A
β, ζ	203.21	38.46	3.19 B
β, σ	191.53	29.45	3.19 C
β, g	202.42	39.74	3.19 D
ζ, σ	198.37	35.98	3.19 E
ζ, g	239.12	70.73	B.16 D
σ, g	199.79	37.30	3.19 F

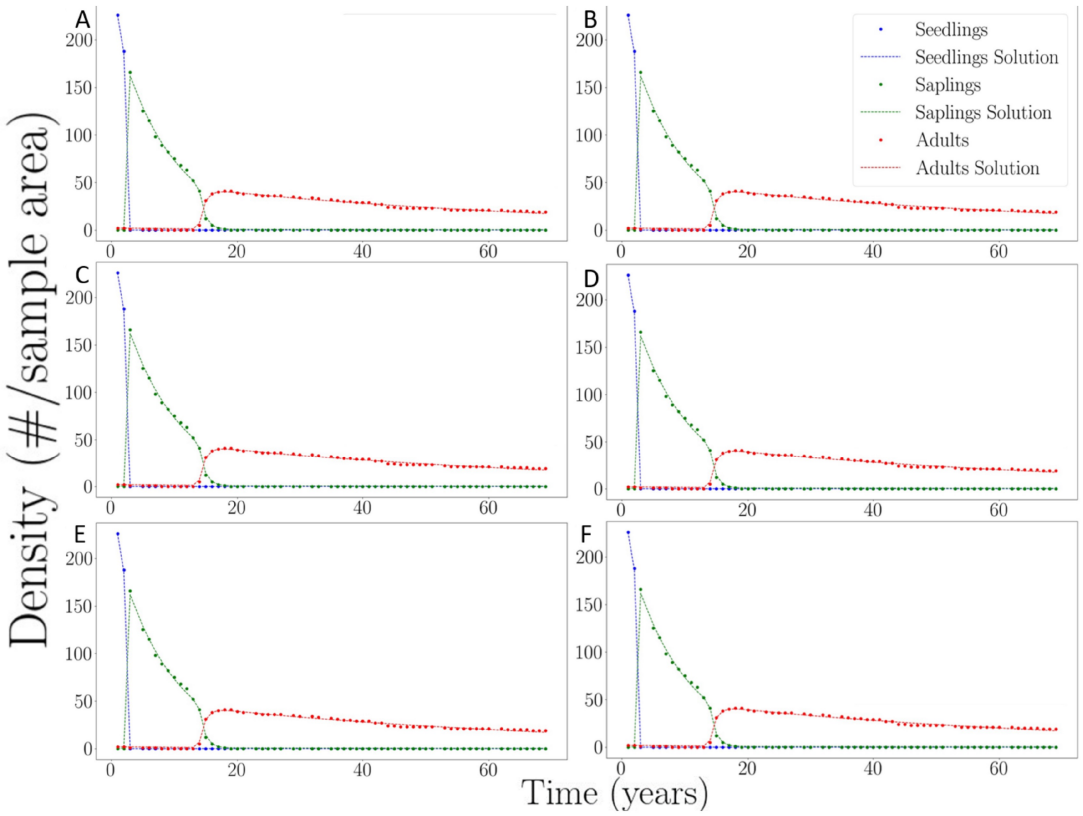

Figure 3.19: Model 7 solution curves following the replacement of the parameters ζ, σ, and g (A), β and ζ (B), β and σ (C), β and g (D), ζ and σ (E), and σ and g (F).

3.3.4.4 Distance from Edge Ecological Results from Model 7

Model 7 indicated significant edge influence on shade-intolerant tree populations from 0 m - 10 m into the interior forest. At distances further than 10 m from the edge, the model reported a declining shade-intolerant seedling, sapling, and adult tree populations. Edge influence on shade-intolerant trees from 0 m - 10 m from the edge decreased over time. Model results indicated that the most significant changes to the seedling and sapling populations occurred within the first 5 years. After 5 years, seedling and sapling populations began to dramatically decline. At approximately 15 years, the adult population began to increase, and remained above 0 for the duration of the model simulation.

The results for Model 7 indicate that this model was able to accurately capture population behaviour produced by SORTIE-ND between 0 m - 10 m from the clear cut harvest (Figure 3.20). From 10 m - 20 m, I observed that the magnitude of the populations of seedlings, saplings, and adult shade-intolerant trees was significantly less than those observed at the edge (Figure 3.20 B). For 10 m - 20 m and 20 m - 30 m from the edge, the magnitude of the populations was so small that it was not reasonable to attempt to fit the model to these data (Figure 3.20 B-C).

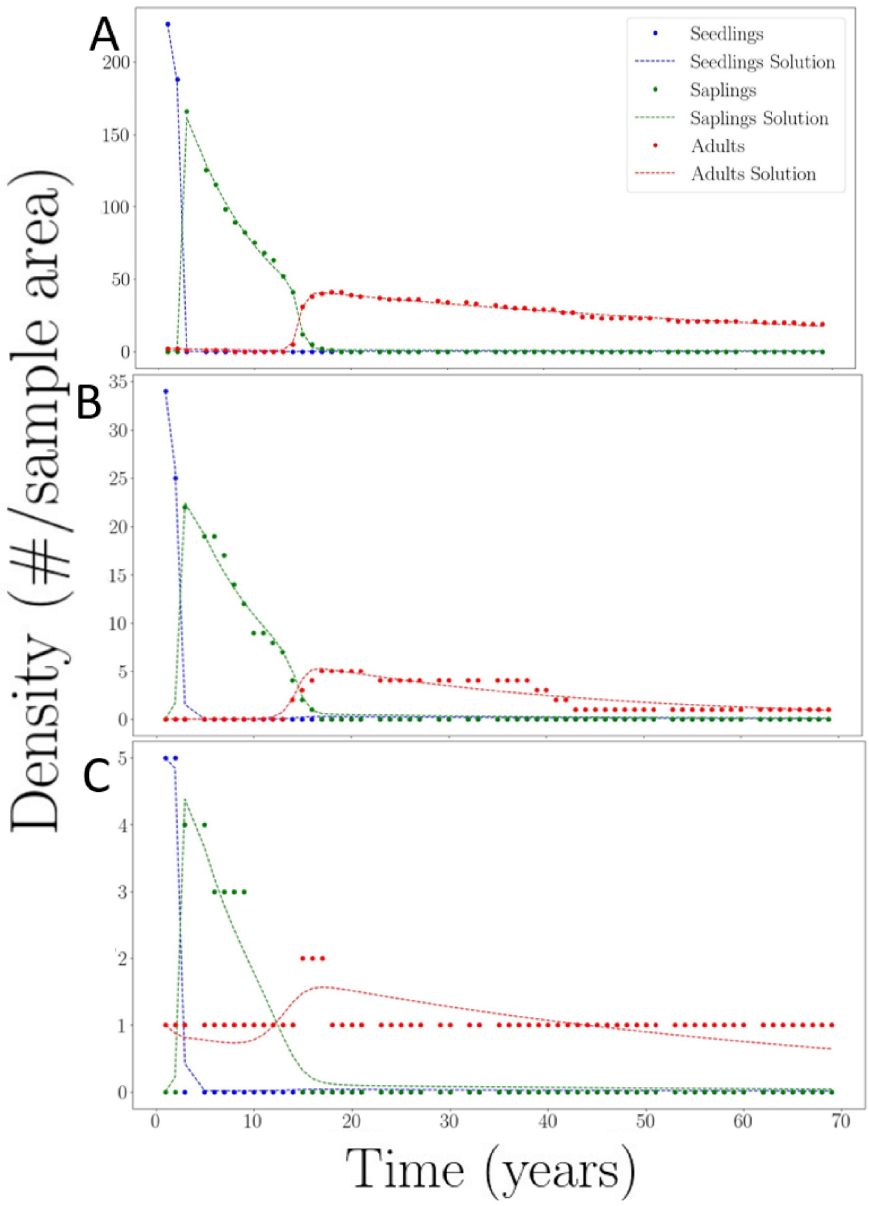

Figure 3.20: Model 7 fitting results for the population trends of seedlings, saplings, and adults at varying distances from the edge: 0 m - 10 m (A), 10 m - 20 m (B), and 20 m - 30 m (C).

3.4 Discussion

Using the simulated SORTIE-ND dataset, my objective was to construct temporal ODE based mathematical models capable of describing the population dynamics of shade-intolerant trees following the creation of a clear-cut edge. Drawing inspiration from the foundational framework of the SIR compartmental model, I developed a set of eight nested ODE models. Among these models, one particular candidate, Model 7, was selected for further examination.

Model 7 incorporated crucial improvements in the form of time-dependent relationships introduced to the seedling mortality rate, seedling maturation rate, and sapling maturation rate, effectively capturing key dynamics observed between the populations. Sensitivity analyses of Model 7 uncovered that only a subset of its parameters/coefficients demonstrated sensitivity to noise in the data. The adult population was identified as the most sensitive to changes in best-fit parameter/coefficient values. Notably, even slight variations in these parameter and coefficient values had a cumulative effect, resulting in more substantial population changes that became evident in later generations. The parameters/coefficients that elicited a sensitive response from the seedling, sapling, and adult populations tended to be associated with significant biological functions such as the seedling establishment, sapling and adult death rates, and the average times of maturation. The coefficients, σ and h, which appear in the time-dependent expressions for c_2 and μ_1 (eq. 3.7b and eq. 3.6a), played a critical role in the fluctuation observed in the adult population. For each of these parameters, these coefficients have a significant influence on the value of the parameter at a given time, t. Given the structure of these parameters, even small variations in these coefficient values can lead to substantial differences in the final parameter value. As such,

these coefficient sensitivity results agree with the structure of Model 7.

An exploration of the structure Model 7 led to the identification of four parameters/coefficients that could potentially be considered redundant. Remarkably, removing some combinations of these parameters resulted in improved SSE and AIC values compared to that of the original model, suggesting a refined and more streamlined model structure. The structure test identified β as one of the four redundancies in the model. The results of parameter/coefficient fitting reported β's best-fit value as 6.2432×10^{-2}. Given the magnitude of this estimate, it is unsurprising that replacing this parameter with 0 did not have significant influence on Model 7's AIC and SSE scores. However, it is important to consider that while β is apparently redundant given the simulated data, the parameter signifies a biological process within an ecological system. As such the complete removal of this parameter from future iterations of the model may not be reflective of a true ecological system. The remaining coefficients, σ (eq. 3.7b), ζ (eq. 3.7b), and g (eq. 3.6a), all correspond to fitted coefficients in the parameters c_2 and μ_2. From the best-fit values, we observe that σ, g, and ζ are all relatively close to their replacement values (Table 3.4). As such, removing the requirement of fitting these three coefficients and replacing these terms with a constant value close to their estimated best-fit value resulting in improved SSE and AIC scores is not entirely unexpected.

Finally, I sought to assess the capability of Model 7 to describe changes in shade-intolerant tree populations at varying distances from the edge. By examining distances further from the edge, it can better understood how spatial dynamics impact model behaviour. Unfortunately, the results we used from SORTIE-ND yielded such a small amount of data for further distances from the edge that is was not reasonable to do any

further model fitting. However, this is not completely unexpected. The boreal forest we simulated in SORTIE-ND aligns with the results generally reported within existing literature. Results of empirical edge studies often report diminished impact of edge influence on boreal forests interior regions, which was reflected in the shade-intolerant tree populations in the simulated system (Harper et al., 2005, 2015).

3.4.0.1 Forest Population Models

Model 7 described a system in which seedling mortality, seedling maturation, and sapling maturation rates are defined as time-dependent functions. The structure of these parameters define these rates as specific to a developmental period for shade-intolerant trees. In forest population modelling, the concept of changing rates given a categorization of the life stage of a tree is not an uncommon notion (Condit et al., 1998). Many population models such as Condit et al. (1999), use stage structure to inform mortality and growth rates. However, many models such as the Chapman-Richards generalization of Von Bertalanffy's Growth Model, inform mortality and maturation rates given a categorization of size structure, specifically diameter (Pienaar & Turnbull, 1973). Comparatively, Model 7 generalizes these measurements by categorizing the stand population into three age-structured compartments. A similar approach was taken by Condit et al. (1998), where trees were classified and examined based on their diameter. In contrast, I removed the requirement of specifying a DBH (diameter at breast height) measurement for each tree and instead classified growth and mortality rates as seedling, sapling, or adult specific parameters. Given the results of the data fitting, this generalization procedure appears to be an efficient way of defining tree mortality and maturation rates for varying developmental stages of shade-intolerant trees.

In my models, I categorized shade-intolerant trees into three population classes, seedlings, saplings, and adults, an age classification of trees sometimes found in empirical edge studies (e.g. Krishnadas et al., 2019). Parameters are based on these three compartments. This model structure is based on the SIR compartmental structure often associated with the spread of pathogens (Kermack et al., 1997). While the SIR model has been considered advantageous to forest ecological research in such areas as forest pathogens (e.g. Dobson & Crawley, 1994), forest insect outbreaks (e.g. Liebhold et al., 2004), and fire ecology (e.g. Hébert-Dufresne et al., 2018), this model structure has yet to be considered in the field of edge research. Furthermore, while my models present an age compartmental model structure, other compartmental models in forest ecology differ in structural composition. For instance, Hébert-Dufresne et al. (2018) employed a burning, growth, and thinning (BGT) compartmental model to characterize forest fire spread in tropical regions. In contrast, Condit et al. (1998) adopted diameter size classes, delineating a total of fourteen distinct compartments in their study.

3.4.0.2 Forest Edge Models

The creation of an edge often elicits varying degrees of vegetation responses. Empirical boreal edge studies suggest that increases in seedling and sapling populations are often recorded as initial responses to clear-cut edges (Burton, 2002; Harper et al., 2015, 2016; Harper & Macdonald, 2002). Model 7 indicates a remarkable capability of reproducing SORTIE-ND observed vegetation responses for both short-term and long-term time scales. Forest harvest models possess similar prediction capabilities as Model 7, with most models indicating an increase in both shade-intolerant seedling and saplings immediately post-harvest (e.g. Arseneault & Saunders, 2012 and Raymond et al.,

2016). Following harvest, many models also suggest a significant increase in shade-intolerant seedling and sapling mortality (Arseneault & Saunders, 2012; Raymond et al., 2016). We observed the same trends in the SORTIE-ND simulation data and as such, incorporated these dynamics into Model 7.

The applicability of Model 7 decreased farther away from the edge. This was due to the considerable decrease in these data farther away from the edge. It is generally found within edge literature that boreal forests are characterized by having weaker responses to edge influence (Harper et al., 2005, 2015). As the SORTIE-ND simulation parameter file corresponded to an eastern Canadian boreal mixed-wood system and the population data focusing on shade-intolerant tree populations, it is unsurprising that the magnitude of data for these tree species significantly decreased further into the plot. While Model 7 was trained and tested on a system describing a boreal forest, applying the model structure to non-boreal data may yield different results. For example, tropical forests often exhibit edge responses at distances as far as hundreds of metres into the interior forest (Laurance et al., 2002). As such, applying Model 7 to a clear-cut edge data of a tropical forest may allow for the model to identify edge influence further into the interior forest, given there are sufficient data. Additionally, while my simulated data consisted of a clear-cut edge creation, Model 7's structure maintains the ability to examine edge effects of varying edge types. In turn, Model 7 has the capability to explore shade-intolerant tree responses to varying edge creations and possibly within other biomes.

Chapter 4

Conclusion and Future Work

4.1 Summary of Results

The forest simulator SORTIE-ND offered an effective and easily accessible solution for generating a substantial dataset, which proved instrumental for the design and testing of my ODE models. Using a pre-built parameter file from Bose et al. (2015), I successfully simulated 100 years of boreal forest growth following a clear-cut harvest. The simulation's output highlighted notable changes in shade-intolerant tree populations in response to the creation of an edge. To focus my analysis, I filtered out the shade-tolerant tree population from the dataset, concentrating solely on the shade-intolerant trees. From this simulation, I was able to collect 63 time-steps of usable population data for structuring and fitting my models.

The primary objective of this research was to develop a system of age-structured ODE models capable of describing the dynamics of shade-intolerant tree populations at various distances from the edge after a clear-cut harvest. To achieve this, I adapted and modified the SIR framework originally presented by Kermack et al. (1997), tailoring it to represent an age-structured forest population. By introducing time-dependent

parameters, I constructed eight nested models, each of which was fitted to the simulated data and evaluated based on their SSE and AIC scores. After this analysis, Model 7 was identified as the most suitable candidate. This model incorporated three essential time-dependent parameters: a seedling maturation rate, a sapling maturation rate, and a seedling mortality rate. To further investigate the model's robustness and predictive power, I performed various sensitivity analyses on Model 7. The analyses demonstrated that a small subset of Model 7's parameters were sensitive to noise in the data. Furthermore, upon introducing noise into parameter estimate, the adult solution curve proved to be the most sensitive of the three age-structure populations. Finally, the structure test revealed a subset of parameters and coefficients that were redundant in the model. The model's SSE and AIC scores were demonstrably better than those of the original model. These analyses provided insights into the model's reliability and confidence in predictions.

The solution curves of Model 7 demonstrated a precise fit to the simulated data within the range of 0 m - 10 m from the edge. The population trends within this distance range were accurately represented by the model. However, for data points beyond 10 m up to 30 m, the sample size was insufficient to attempt to fit the model. Consequently, I could not draw definitive conclusions about the model's predictive capabilities regarding edge influence beyond 10 m from the edge. However, it would be straightforward to address this simply by running SORTIE-ND with a larger tree population. This would yield a sufficiently large tree population beyond 10 m from the edge that would allow the modelling techniques considered in this thesis to be employed. Temporally, both the data and the model results suggested that edge influence on populations near the edge tended to stabilize after 40 years. It is important to note that

the harvested edge was not maintained post-harvest, and this could have contributed to the levelling out of shade-intolerant populations. Moreover, shade-intolerant tree populations adjacent to a maintained edge may exhibit different responses.

4.2 Key Results

The performance of Model 7 indicates that it is possible to adapt a structural framework of an SIR model and, by applying time-dependencies to the parameters, describe a shade-intolerant tree forest population at a harvested edge. By observing the time-dependent relationship between seedling and sapling populations and their subsequent maturation and mortality rates, I showed that by using a hierarchical model framework, with each model incorporating a higher-level of parameter complexity than the last, it is possible to accurately describe the population dynamics present in the data and identify which parameters are best described using more complex, time-dependent equations.

For this system, I constructed eight ODE models of varying levels of complexity, designed to describe the population trends of shade-intolerant trees observed from a simulated data set. Model 7, which incorporated improvements to the seedling mortality rate, seedling maturation rate, and sapling maturation rate, was not the most complex model of the cohort. Model 7's identification as the best model using the AIC selection criteria suggests that the parameter selection for this model strikes the appropriate balance between goodness of fit and model complexity. Model 8, which included the improvement of the seedling maturation rate, seedling mortality rate, sapling maturation rate, and sapling mortality rate, performed comparably to Model 7. However, Model 8, which included the improved sapling mortality, yielded a slightly higher SSE score than that of Model 7. This suggests that despite incorporating

all proposed time-dependent parameters, Model 8 still underperformed compared to Model 7. Even though there appeared to be an observable time-dependent relationship between time and sapling mortality, this idea was not supported by the SSE or the AIC scores.

Furthermore, while I constructed a model cohort by incorporating higher-level changes in each model iteration, I identified possible redundancies present in Model 7 by fine-tuning parameter functions through testing the structural composition of the model. By isolating parameter and coefficient values and replacing them with constant coefficients, I identified six simplified model variations that produced smaller SSE and AIC values. Of these six sub-models, two sub-models removed coefficient terms not specifically representing any particular biological process present in the model. Given these results, it is clear that the framework implemented to conduct the model development and sensitivity test is not only applicable to the development and construction of a model representing an ecological system, but can also identify redundancies in model structure that could lead to improved model fitting capabilities, and model parameter structures specified to the observed system.

Finally, it is notable that SORTIE-ND provided an accessible and relatively accurate means to simulate longitudinal data in the absence of empirically observed data. The forest simulator was designed with inherent flexibility in mind to allow users to create parameter files of any forest stand, with built-in disturbances and harvest behaviours that can replicate an impressive range of possible scenarios that could be introduced to a system. However, while this tool is an accessible option, designing parameter files that incorporate accurate measurements reflective of the stand being represented is complex. By using a pre-written parameter file, I was able to simulate

the boreal forest stand and introduce new behaviours without the added challenge of initializing the stand. However, for stands in which parameter files are yet to be completed, constructing the parameter file to simulate in the simulator would prove an extensive amount of effort.

4.3 Model Limitations

Gathering empirical data for numerical parameter and coefficient values posed a significant challenge due to limited longitudinal edge studies and varying vegetation responses across different studies. The existing literature lacked sufficient amounts of field data over time to accurately test complex mathematical models. To avoid overfitting and to achieve accurate parameter fitting, I required a much larger dataset than what was available. To address this, I opted for a simulated dataset using the flexible SORTIE-ND forest simulator. This allowed me to design a clear-cut edge system and observe changes in shade-intolerant tree populations over an extended time. The simulation provided comprehensive data, including individual seedling information, which are often not available in empirical studies. However, using a simulated dataset comes with limitations. The ODE models may be influenced by the simulation's core assumptions and underlying relationships, potentially introducing bias. Empirical data remains preferable due to the more reliable nature.

In this research, I utilized an ODE model based on the SIR compartmental framework. Despite its suitability for my purposes, ODE models have inherent limitations compared to other model types. One constraint is their limitation to a single independent variable. Considering my focus on shade-intolerant tree responses, I chose time as the independent variable, as long-term evaluations of edge influence is often challenging in empirical studies. While time is crucial, distance also plays a signifi-

cant role in evaluating edge influence on vegetation responses. Although I could not directly incorporate distance as an independent variable, I attempted to assess the model's performance using subsets of data at various distances from the edge. However, data limitations beyond 10 m limited the model's fitting accuracy. Consequently, a definitive conclusion on the model's capability to estimate DEI remains inconclusive.

Another notable limitation of the model is the specificity of the data used for its construction and testing. The model was developed based on simulated shade-intolerant tree population data obtained from a SORTIE-ND parameter file representing a *Populus tremuloides* Michx-dominated stand in eastern Canada. Time-dependent parameters were incorporated into the model dynamics based on trends observed in this particular dataset. Consequently, the model's applicability to different systems, tree types, or vegetation remains uncertain. It may have limited capability to describe trends beyond this specific system. Further investigations could explore varying systems and tree species to assess the model's generalizability. Additional testing is required to establish the scope of systems this model can effectively describe.

4.4 Future Research

While simulated data offers an accessible means of data collection, constructing and testing models with true empirical data is generally preferred. Therefore, future edge studies could explore the potential for conducting longitudinal studies on the effects of different edge creation scenarios. Moreover, establishing a universal standard for data collection in various edge studies could enhance overall data availability. Alternatively, to support future model testing and development, efforts could be made to expand the parameter files available to SORTIE-ND. Parameter files for forests with higher biomass, such as temperate or tropical forests (Harper et al., 2005; McWethy

et al., 2009), might yield more substantial vegetation responses. By having diverse SORTIE-ND parameter files at hand, further exploration of mathematical models in edge research can be conducted without the time constraints associated with waiting for field study data collection.

Further exploration of this model's capabilities could involve testing it on various edge types, forest ecosystems, and vegetation. Although initially developed and tested on a specific system, the model's design allows for parameter fitting and adjustment based on observed data trends. Consequently, it may be applicable for testing on shade-intolerant tree populations in different forest and edge settings. However, the model's suitability for describing other vegetation types remains uncertain, as it depends on their unique properties. Vegetation with similar attributes, such as shade-intolerance, could be potential candidates for model application. In contrast, describing shade-tolerant vegetation would require additional investigation to draw definitive conclusions.

To address the interest of edge researchers in understanding the temporal and spatial influences on vegetation, expanding the model from an ODE to a partial differential equation (PDE) framework is recommended. PDE models offer the ability to assess changes with respect to multiple independent variables. In edge research, a PDE model could simultaneously explore edge influence over both time and space. A potential initial step to transition from an ODE to a PDE model is incorporating a seedling dispersal term. Additionally, considering the expansion of time-dependent parameters to include a distance variable would allow spatial locations to influence rates such as establishment, maturation, and mortality. This approach would provide a more comprehensive view of the entire stand and how edges impact the interior

ecosystem.

References

Akaike, H. (1998). Information theory and an extension of the maximum likelihood principle. In E. Parzen, K. Tanabe, & G. Kitagawa (Eds.), *Selected papers of hirotugu akaike* (p. 199–213). New York, NY: Springer. Retrieved from `https://doi.org/10.1007/978-1-4612-1694-0_15` doi: 10.1007/978-1-4612-1694-0_15

Ameztegui, A., Cabon, A., De Cáceres, M., & Coll, L. (2017). Managing stand density to enhance the adaptability of scots pine stands to climate change: A modelling approach. *Ecological Modelling*, *356*, 141–150. doi: 10.1016/j.ecolmodel.2017.04.006

Ameztegui, A., Paquette, A., Shipley, B., Heym, M., Messier, C., & Gravel, D. (2017). Shade tolerance and the functional trait: demography relationship in temperate and boreal forests. *Functional Ecology*, *31*(4), 821–830. doi: 10.1111/1365-2435.12804

Anyomi, K. A., Neary, B., Chen, J., & Mayor, S. J. (2022). A critical review of successional dynamics in boreal forests of north america. *Environmental Reviews*, *30*(4), 563–594. doi: 10.1139/er-2021-0106

Arseneault, J. E., & Saunders, M. R. (2012). Incorporating canopy gap-induced growth responses into spatially implicit growth model projections. *Ecological Modelling*, *237*, 120–131. doi: 10.1016/j.ecolmodel.2012.04.003

Ashraf, M. I., Bourque, C. P., MacLean, D. A., Erdle, T., & Meng, F.-R. (2012). Using JABOWA-3 for forest growth and yield predictions under diverse forest conditions of nova scotia, canada. *Forestry Chronicle*, *88*(6), 708–721.

Benson, D. L., King, E. G., & O'Brien, J. J. (2022). Forest dynamics models for conservation, restoration, and management of small forests. *Forests*, *13*(4), 1-25. doi: 10.3390/f13040515

Bose, A. K., Harvey, B. D., Coates, K. D., Brais, S., & Bergeron, Y. (2015). Modelling stand development after partial harvesting in boreal mixedwoods of eastern canada. *Ecological Modelling*, *300*, 123–136. doi: 10.1016/j.ecolmodel.2015.01.002

Botkin, D. B. (1993). Forest dynamics: An ecological model. In (p. 309). Oxford University Press.

Braithwaite, N. T., & Mallik, A. U. (2012). Edge effects of wildfire and riparian buffers along boreal forest streams: Edge effects of wildfire and riparian buffers. *The Journal of Applied Ecology*, *49*(1), 192–201. doi: 10.1111/j.1365-2664.2011.02076.x

Branch, M. A., Coleman, T. F., & Li, Y. (1999). A subspace, interior, and conjugate gradient method for large-scale bound-constrained minimization problems. *SIAM Journal on Scientific Computing*, *21*(1), 1–23. doi: 10.1137/S1064827595289108

Burnham, K. P., & Anderson, D. R. (2003). *Model selection and multimodel inference: A practical information-theoretic approach.* Springer Science & Business Media.

Burton, P. (2002). Effects of clearcut edges on trees in the sub-boreal spruce zone of northwest-central british columbia. *Silva Fennica*, *36*(1). doi: 10.14214/sf.566

Canham, C. D. (n.d.). *SORTIE-ND software for spatially-explicit simulation of forest dynamics.* Retrieved 2023-04-08, from `http://www.sortie-nd.org/`

Canham, C. D., & Murphy, L. (2017). The demography of tree species response to climate: sapling and canopy tree survival. *Ecosphere*, *8*(2), e01701. doi: 10.1002/ecs2.1701

Casella, G., & Berger, R. L. (2002). *Statistical inference* (No. 2). Thomson Learning.

Chen, J., Franklin, J. F., & Spies, T. A. (1992). Vegetation responses to edge environments in old-growth douglas-fir forests. *Ecological Applications*, *2*(4), 387–396. doi: 10.2307/1941873

Coates, K. D., Canham, C. D., Beaudet, M., Sachs, D. L., & Messier, C. (2003). Use of a spatially explicit individual-tree model (SORTIE/BC) to explore the implications of patchiness in structurally complex forests. *Forest Ecology and Management*, *186*(1), 297–310.

Coates, K. D., Hall, E., Astrup, R., & Henderson, B. (2023). *Final technical report: Fsp project y103187 evaluation of the complex stand simulation model SORTIE-ND for timber supply review in sub-boreal forests of northern bc* (Tech. Rep.). 1188 Main Street, Box 4274, Smithers, British Columbia, V0J 2N0, Canada: Bulkley Valley Centre for Natural Resources Research and Management.

Condit, R., Ashton, P. S., Manokaran, N., LaFrankie, J. V., Hubbell, S. P., & Foster, R. B. (1999). Dynamics of the forest communities at pasoh and barro colorado: Comparing two 50-ha plots. *Philosophical Transactions: Biological Sciences*, *354*(1391), 1739–1748.

Condit, R., Sukumar, R., Hubbell, S. P., & Foster, R. B. (1998). Predicting population trends from size distributions: A direct test in a tropical tree community. *The American Naturalist*, *152*(4), 495–509. doi: 10.1086/286186

Didham, R. K., Kapos, V., & Ewers, R. M. (2012). Rethinking the conceptual foundations of habitat fragmentation research. *Oikos*, *121*(2), 161–170. doi: 10.1111/j.1600-0706.2011.20273.x

Didham, R. K., & Lawton, J. H. (1999). Edge structure determines the magnitude of changes in microclimate and vegetation structure in tropical forest fragments1. *Biotropica*, *31*(1), 17–30. doi: 10.1111/j.1744-7429.1999.tb00113.x

Dobson, A., & Crawley, M. (1994). Pathogens and the structure of plant communities. *Trends in Ecology & Evolution*, *9*(10), 393–398. doi: 10.1016/0169-5347(94)90062-0

Esseen, P.-A., Hedstrom Ringvall, A., Harper, K. A., Christensen, P., & Svensson, J. (2016). Factors driving structure of natural and anthropogenic forest edges from temperate to boreal ecosystems. *Journal of Vegetation Science*, *27*(3), 482–492. doi: 10.1111/jvs.12387

Evans, M. R., Bithell, M., Cornell, S. J., Dall, S. R. X., Diaz, S., Emmott, S., ... Benton, T. G. (2013). Predictive systems ecology. , *280*, 1-9. doi: 10.1098/rspb .2013.1452

Ewers, R. M., & Didham, R. K. (2006). Continuous response functions for quantifying the strength of edge effects. *Journal of Applied Ecology*, *43*(3), 527–536. doi: 10.1111/j.1365-2664.2006.01151.x

Franklin, C. M. A., Harper, K. A., & Clarke, M. J. (2021). Trends in studies of edge influence on vegetation at human-created and natural forest edges across time and space. *Canadian Journal of Forest Research*, *51*(2), 274–282. doi: 10.1139/cjfr-2020-0308

Gear, C. W. (1971). Numerical initial value problems in ordinary differential equations. *The Computer Journal*(2). doi: https://doi.org/10.1093/comjnl/15.2.155

Haddad, N. M., Brudvig, L. A., Clobert, J., Davies, K. F., Gonzalez, A., Holt, R. D., ... Townshend, J. R. (2015). Habitat fragmentation and its lasting impact on earth's ecosystems. *Science Advances*, *1*(2), 1-9. doi: 10.1126/sciadv.1500052

Harper, K. A., Drapeau, P., Lesieur, D., Bergeron, Y., & Verheyen, K. (2016). Negligible structural development and edge influence on the understorey at 16–17-yr-old clear-cut edges in black spruce forest. *Applied Vegetation Science*, *19*(3), 462–473. doi: 10.1111/avsc.12226

Harper, K. A., & Macdonald, S. E. (2002). Structure and composition of edges next to regenerating clear-cuts in mixed-wood boreal forest. *Journal of Vegetation Science*, *13*(4), 535–546. doi: 10.1111/j.1654-1103.2002.tb02080.x

Harper, K. A., MacDonald, S. E., Burton, P. J., Chen, J., Brosofske, K. D., Saunders, S. C., ... Esseen, P.-A. (2005). Edge influence on forest structure and composition in fragmented landscapes. *Conservation Biology*, *19*(3), 768-782. doi: https://doi.org/10.1111/j.1523-1739.2005.00045.x

Harper, K. A., Macdonald, S. E., Mayerhofer, M. S., Biswas, S. R., Esseen, P.-A., Hylander, K., ... Bergeron, Y. (2015). Edge influence on vegetation at natural

and anthropogenic edges of boreal forests in canada and fennoscandia. *Journal of Ecology*, *103*(3), 550–562.

Hindmarsh, A. (1992). Odepack. a collection of ode system solvers. , *1*, 55-64. Retrieved from `https://www.osti.gov/biblio/145724`

Hofmeister, J., Hošek, J., Brabec, M., Střalková, R., Mýlová, P., Bouda, M., ... Svoboda, M. (2019). Microclimate edge effect in small fragments of temperate forests in the context of climate change. *Forest Ecology and Management*, *448*, 48–56. doi: 10.1016/j.foreco.2019.05.069

Huth, A., Ditzer, T., & Bossel, H. (1998). *The rain forest growth model FORMIX3: Model description and analysis of forest growth and logging scenarios for the deramakot forest reserve (malaysia).* Goltze.

Hébert-Dufresne, L., Pellegrini, A. F. A., Bhat, U., Redner, S., Pacala, S. W., & Berdahl, A. M. (2018). Edge fires drive the shape and stability of tropical forests. *Ecology Letters*, *21*(6), 794–803. doi: 10.1111/ele.12942

Iooss, B., & Lemaître, P. (2015). A review on global sensitivity analysis methods. In G. Dellino & C. Meloni (Eds.), (p. 101–122). Springer US. doi: 10.1007/978-1-4899-7547-8_5

Keenan, R., & Kimmins, J. (1993). The ecological effects of clear-cutting. *Envrionmental Review*, *1*, 121–144. doi: 10.1139/a93-010

Kermack, W. O., McKendrick, A. G., & Walker, G. T. (1997, Jan). A contribution to the mathematical theory of epidemics. *Proceedings of the Royal Society of London.*

Series A, Containing Papers of a Mathematical and Physical Character, *115*(772), 700–721. doi: 10.1098/rspa.1927.0118

Kimmins, J. P. (2003). *Forest ecology* (3rd edition ed.). Pearson.

Krishnadas, M., Kumar, A. N., & Comita, L. S. (2019). Edge effects reduce α-diversity but not β-diversity during community assembly in a human-modified tropical forest. *Ecological Applications*, *29*(8), 1–10.

Laurance, W. F., Lovejoy, T. E., Vasconcelos, H. L., Bruna, E. M., Didham, R. K., Stouffer, P. C., ... Sampaio, E. (2002). Ecosystem decay of amazonian forest fragments: a 22-year investigation. *Conservation Biology*, *16*(3), 605–618. doi: 10.1046/j.1523-1739.2002.01025.x

Leemans, R., & Prentice, I. C. (1989). FORSKA, a general forest succession model. In (p. 70). Växtbiologiska inst.

Levenberg, K. (1944). A method for the solution of certain non-linear problems in least squares. *Quarterly of Applied Mathematics*, *2*(2), 164–168. doi: 10.1090/qam/10666

Lexer, M. J., & Hönninger, K. (1998). Simulated effects of bark beetle infestations on stand dynamics in picea abies stands: coupling a patch model and a stand risk model. *Lecture Notes in Earth Sciences, Berlin Springer Verlag*, *74*, 289–308. doi: 10.1007/BFb0009780

Liebhold, A., Koenig, W. D., & Bjørnstad, O. N. (2004). Spatial synchrony in population dynamics. *Annual Review of Ecology, Evolution, and Systematics*, *35*(1), 467–490. doi: 10.1146/annurev.ecolsys.34.011802.132516

Lourakis, M. (2005). A brief description of the levenberg-marquardt algorithm implemened by levmar. *A Brief Description of the Levenberg-Marquardt Algorithm Implemented by Levmar*, *4*.

McWethy, D. B., Hansen, A. J., & Verschuyl, J. P. (2009). Edge effects for songbirds vary with forest productivity. *Forest ecology and management*, *257*(2), 665–678. doi: 10.1016/j.foreco.2008.09.046

Menard, A., Dube, P., Bouchard, A., Canham, C. D., & Marceau, D. J. (2002). Evaluating the potential of the SORTIE forest succession model for spatio-temporal analysis of small-scale disturbances. *Ecological Modelling*, *153*(1–2), 81–96. doi: 10.1016/S0304-3800(01)00503-8

Mitchell, S. J., Hailemariam, T., & Kulis, Y. (2001). Empirical modeling of cutblock edge windthrow risk on vancouver island, canada, using stand level information. *Forest Ecology and Management*, *154*(1), 117–130. doi: 10.1016/S0378-1127(00)00620-4

Moran, E., Vannest, N., & Aubry-Kientz, M. (2021). Modeling the forest dynamics of the sierra nevada under climate change using SORTIE-ND. *Annals of Forest Science*, *78*(3), 75. doi: 10.1007/s13595-021-01074-z

Morozov, A. (2013). Mathematical modelling in theoretical ecology: Introduction to the special issue. *Mathematical Modelling of Natural Phenomena*, *8*(6), 1–4. doi: 10.1051/mmnp/20138601

Murcia, C. (1995). Edge effects in fragmented forests - implications for conservation. *Trends in Ecology & Evolution*, *10*(2), 58–62. doi: 10.1016/S0169-5347(00)88977-6

Optimization and root finding (scipy.optimize) — scipy v1.8.0 manual. (n.d.). Retrieved 2022-03-30, from https://docs.scipy.org/doc/scipy/reference/generated/scipy.optimize.least_squares.html

Payne, N. J. (2019). Boreal mixedwood forest potential for carbon uptake and storage. *Frontline Express*(84).

Petzold, L. (1983). Automatic selection of methods for solving stiff and nonstiff systems of ordinary differential equations. , *4*, 136–148. doi: 10.1137/0904010

Pienaar, L. V., & Turnbull, K. J. (1973). The chapman-richards generalization of von bertalanffy's growth model for basal area growth and yield in even - aged stands. *Forest Science*, *19*(1), 2–22.

Poepperl, F., & Seidl, R. (2021). Effects of stand edges on the structure, functioning, and diversity of a temperate mountain forest landscape. *Ecosphere*, *12*(8). doi: 10.1002/ecs2.3692

Radhakrishnan, K., & Hindmarsh, A. C. (1993). *Description and use of lsode, the livermore solver for ordinary differential equations.* Retrieved from https://ntrs.nasa.gov/citations/19940030753

Ranganathan, A. (2004). The levenberg-marquardt algorithm. *Tutoral on LM algorithm*, *11*(1), 101-110.

Raymond, P., Prévost, M., & Power, H. (2016). Patch cutting in temperate mixedwood stands: What happens in the between-patch matrix? *Forest Science*, *62*(2), 227–236. doi: 10.5849/forsci.15-023

Razavi, S., & Gupta, H. V. (2015). What do we mean by sensitivity analysis? the need for comprehensive characterization of "global" sensitivity in earth and environmental systems models. *Water Resources Research*, *51*(5), 3070–3092. doi: 10.1002/2014WR016527

Read, M. N., Alden, K., Timmis, J., & Andrews, P. S. (2020). Strategies for calibrating models of biology. , *21*, 24–35. doi: 10.1093/bib/bby092

Reinmann, A. B., & Hutyra, L. R. (2017). Edge effects enhance carbon uptake and its vulnerability to climate change in temperate broadleaf forests. *Proceedings of the National Academy of Sciences - PNAS*, *114*(1), 107–112. doi: 10.1073/pnas.1612369114

Richardson, J., Cooke, J. E., Isebrands, J. G., Thomas, B. R., & Van Rees, K. C. (2007). Poplar research in canada — a historical perspective with a view to the future. *Canadian Journal of Botany*, *85*(12), 1136–1146. doi: 10.1139/B07-103

Ries, L., Fletcher, R. J., Battin, J., & Sisk, T. D. (2004). Ecological responses to habitat edges: Mechanisms, models, and variability explained. , *35*, 491–522. doi: 10.1146/annurev.ecolsys.35.112202.130148

Ries, L., & Sisk, T. D. (2004). A predictive model of edge effects. *Ecology (Durham)*, *85*(11), 2917–2926. doi: 10.1890/03-8021

Rossi, R., Murari, A., Gaudio, P., & Gelfusa, M. (2020). Upgrading model selection criteria with goodness of fit tests for practical applications. *Entropy*, *22*(4), 447. doi: 10.3390/e22040447

Ruffell, J., & Didham, R. K. (2016). Towards a better mechanistic understanding of edge effects. *Landscape ecology*, *31*, 2205–2213. doi: 10.1007/s10980-016-0397-3

Saltelli, A., Ratto, M., Andres, T., Campolongo, F., Cariboni, J., Gatelli, D., ... Tarantola, S. (2008). *Global sensitivity analysis. the primer* (Vol. 304). doi: 10.1002/9780470725184.ch6

Schroers, B. J. (2011). *Ordinary differential equations: a practical guide.* Cambridge University Press.

Schtickzelle, N., & Baguette, M. (2003). Behavioural responses to habitat patch boundaries restrict dispersal and generate emigration-patch area relationships in fragmented landscapes. *Journal of Animal Ecology*, *72*(4), 533–545. doi: 10.1046/j.1365-2656.2003.00723.x

Scipy. (n.d.). Retrieved 2022-09-2022, from `https://scipy.org`

scipy.integrate.odeint — scipy v1.9.3 manual. (n.d.). Retrieved 2022-12-09, from `https://docs.scipy.org/doc/scipy/reference/generated/scipy.integrate.odeint.html`

Shampine, L. F., & Gear, C. W. (1976). User's view of solving stiff ordinary differential equations. , *21*(1). Retrieved from `https://www.osti.gov/biblio/7327371`

Shao, G., & Shugart, H. (1995). A role-type model (rope) and its application in assessing climate change impacts on forest landscapes. *Vegetation*, *121*(1), 135-146.

Soubeyrand, M., Gennaretti, F., Blarquez, O., Bergeron, Y., Taylor, A. ., L, D., & Marchand, P. (2023). Competitive interactions under current climate allow tem-

perate tree species to grow and survive in boreal mixedwood forest. *Ecography*, *2023*(5), 1-24. doi: 10.1111/ecog.06525

Stroud, A. H. (1974). Initial value problems for ordinary differential equations. In *Numerical quadrature and solution of ordinary differential equations: A textbook for a beginning course in numerical analysis* (p. 207–303). Springer. Retrieved from https://doi.org/10.1007/978-1-4612-6390-6_4

Thom, D., Rammer, W., Dirnböck, T., Müller, J., Kobler, J., Katzensteiner, K., ... Mori, A. (2017). The impacts of climate change and disturbance on spatio-temporal trajectories of biodiversity in a temperate forest landscape. *The Journal of Applied Ecology*, *54*(1), 28–38. doi: 10.1111/1365-2664.12644

Thomas, J. W., Maser, C., & Rodiek, J. E. (1979). Wildlife habitats in managed forests the blue mountains of oregon and washington. agriculture handbook no. 553. u.s. In J. W. Thomas (Ed.), (p. 48-59). Department of Agriculture, Forest Service.

Turner, M. G., Romme, W. H., Gardner, R. H., O'Neill, R. V., & Kratz, T. K. (1993). A revised concept of landscape equilibrium: Disturbance and stability on scaled landscapes. *Landscape Ecology*, *8*(3), 213–227. doi: 10.1007/BF00125352

Urban, D. L. (1990). *A versatile model to simulate forest pattern: A user's guide to zelig version 1.0.* University of Virgina, Environmental Sciences Department.

Urban, D. L., Acevedo, M. F., & Garman, S. L. (1999). Spatial modeling of forest landscape changes. In (chap. Scaling Fine-Scale Processes to Large-Scale Patterns Using Model Derived from Models: Meta-Models). Cambridge.

Vanclay, J. (2006). Forest growth and yield modeling.. doi: 10.1002/9780470057339 .vaf011

Wagenmakers, E.-J., & Farrell, S. (2004). AIC model selection using akaike weights. *Psychonomic Bulletin & Review*, *11*(1), 192–196. doi: 10.3758/BF03206482

Wales, B. A. (1972). Vegetation analysis of north and south edges in a mature oak-hickory forest. *Ecological Monographs*, *42*(4), 451–471. doi: 10.2307/1942167

Yuan, Y.-x. (1999). A review of trust region algorithms for optimization. *ICM99: Proceedings of the Fourth International Congress on Industrial and Applied Mathematics*.

Appendix A

Model Development

Table A.1: Model 1's best-fit coefficients and parameter values.

Parameter/Coefficient	Best-fit Value
β	1.4971×10^{2}
c_1	4.2343×10^{-1}
c_2	4.0066×10^{-35}
μ_1	6.3147×10^{-1}
μ_2	1.3896×10^{-1}
μ_3	1.8387×10^{0}

Table A.2: Model 2's best-fit coefficients and parameter values.

Parameter/Coefficient	Best-fit Value
β	1.5816×10^{1}
c_1	4.742×10^{-1}
c_2	3.9722×10^{-35}
f	1.6148×10^{-11}
g	2.5768×10^{0}
h	1.5761×10^{-1}
μ_2	1.5969×10^{-1}
μ_3	1.6872×10^{0}

Table A.3: Model 3's best-fit coefficients and parameter values.

Parameter/Coefficient	Best-fit Value
β	1.8716×10^{0}
α	8.9008×10^{0}
γ	1.0178×10^{2}
t_{c_1}	7.3633×10^{-2}
δ	2.8470×10^{0}
c_2	3.9722×10^{-35}
μ_1	3.4841×10^{1}
μ_2	6.8940×10^{-2}
μ_3	1.9852×10^{-2}

Table A.4: Model 4's best-fit coefficients and parameter values.

Parameter/Coefficient	Best-fit Value
β	4.65685×10^{-1}
α	5.076×10^{0}
γ	5.2978×10^{0}
t_{c_1}	2.4989×10^{0}
δ	1.5444×10^{-2}
c_2	1.9561×10^{-1}
f	3.8652×10^{-1}
g	2.2243×10^{0}
h	5.1376×10^{-2}
μ_2	7.2583×10^{-2}
μ_3	9.1100×10^{-1}

Table A.5: Model 5's best-fit coefficients and parameter values.

Parameter/Coefficient	Best-fit Value
β	8.7095×10^{-1}
α	4.3366×10^{0}
γ	4.9221×10^{0}
t_{c_1}	2.4268×10^{0}
δ	1.2323×10^{-5}
σ	4.3264×10^{-1}
ψ	1.3948×10^{-1}
t_{c_2}	2.0655×10^{0}
ζ	1.0756×10^{-5}
μ_1	7.9527×10^{-2}
μ_2	9.2394×10^{-2}
μ_3	1.0792×10^{0}

Table A.6: Model 6's best-fit coefficients and parameter values.

Parameter/Coefficient	Best-fit Value
β	1.6827×10^{-2}
α	5.5650×10^{0}
γ	5.5499×10^{0}
t_{c_1}	2.5569×10^{0}
δ	2.8992×10^{-2}
c_2	2.0678×10^{-2}
f	1.3822×10^{0}
g	2.9658×10^{0}
h	7.9103×10^{-2}
i	1.6446×10^{0}
j	2.0589×10^{0}
k	1.3413×10^{-1}
μ_3	4.3696×10^{-3}

Table A.7: Model 8's best-fit coefficients and parameter values.

Parameter/Coefficient	Best-fit Value
β	7.7086×10^{-2}
α	6.6897×10^{0}
γ	7.7551×10^{0}
t_{c_1}	2.4428×10^{0}
δ	1.3890×10^{-11}
σ	2.4619×10^{0}
ψ	2.4151×10^{0}
t_{c_2}	1.4719×10^{1}
ζ	1.9680×10^{-13}
f	6.6569×10^{-1}
g	1.8994×10^{0}
h	1.0438×10^{-1}
i	6.9790×10^{-1}
j	8.2088×10^{-1}
k	1.0850×10^{-1}
μ_3	9.0308×10^{-2}

Appendix B

Sensitivity Analyses

B.1 Parameter/Coefficient Sensitivity Analysis

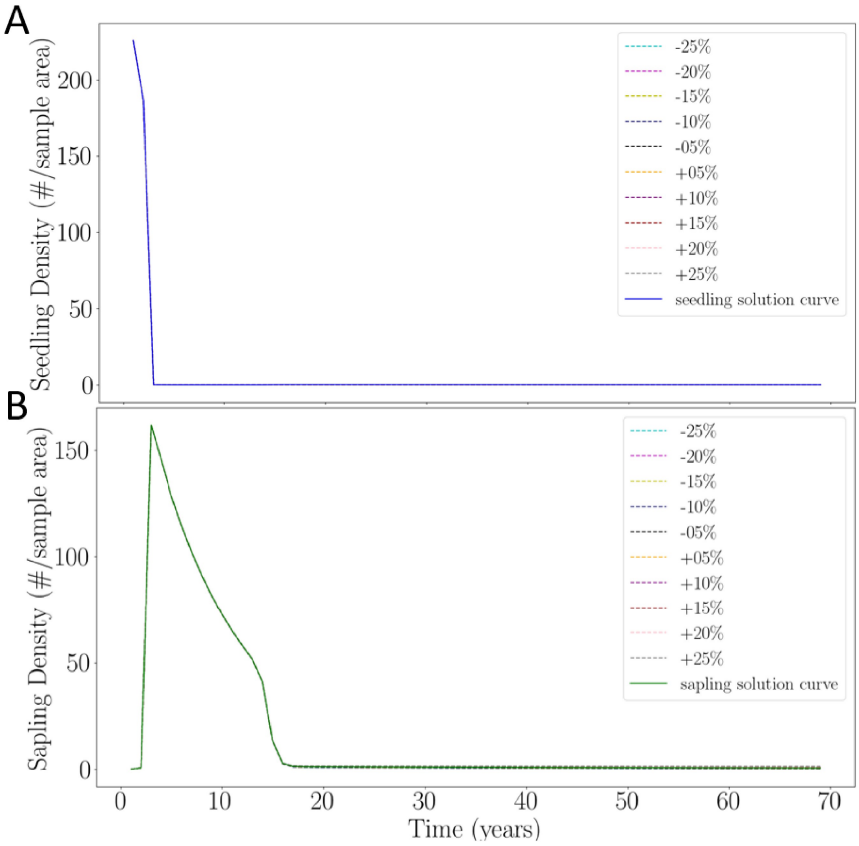

Figure B.1: Parameter sensitivity results for the seedling population (A) and sapling population (B) after perturbing the parameter β.

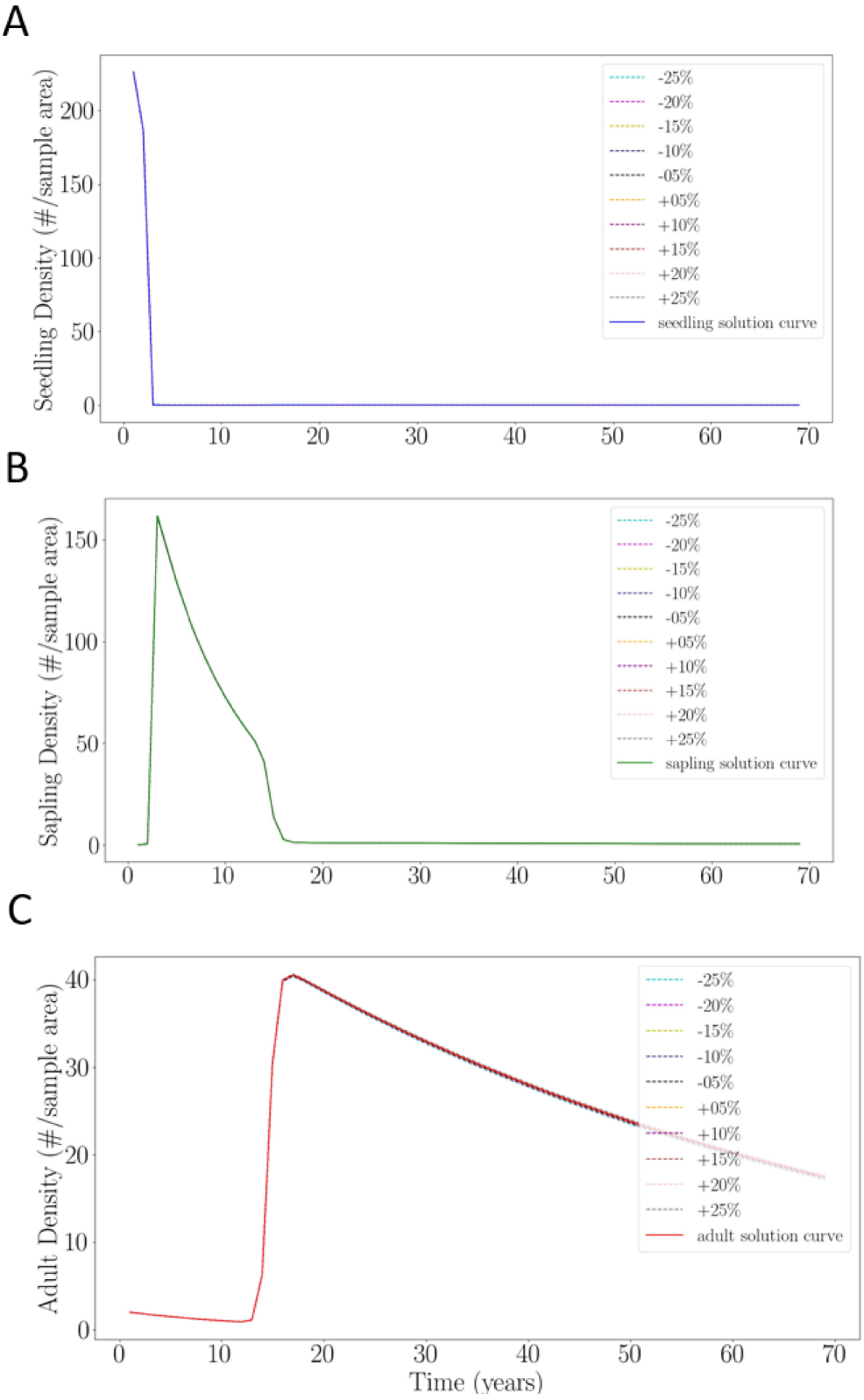

Figure B.2: Coefficient sensitivity results for the seedling (A), sapling (B), and adult populations after perturbing the coefficient α.

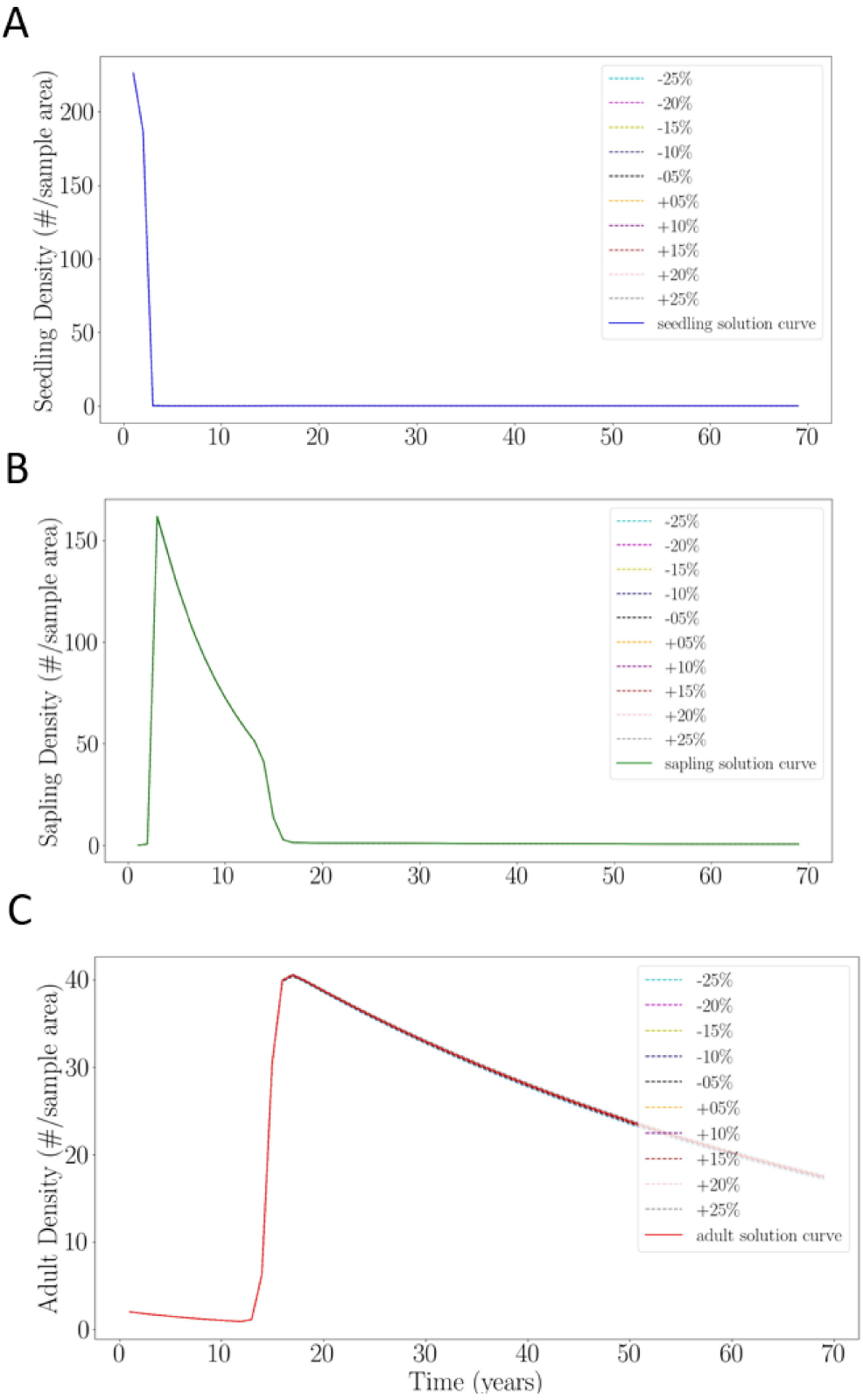

Figure B.3: Coefficient sensitivity results for the seedling (A), sapling (B), and adult (C) populations after perturbing the coefficient γ.

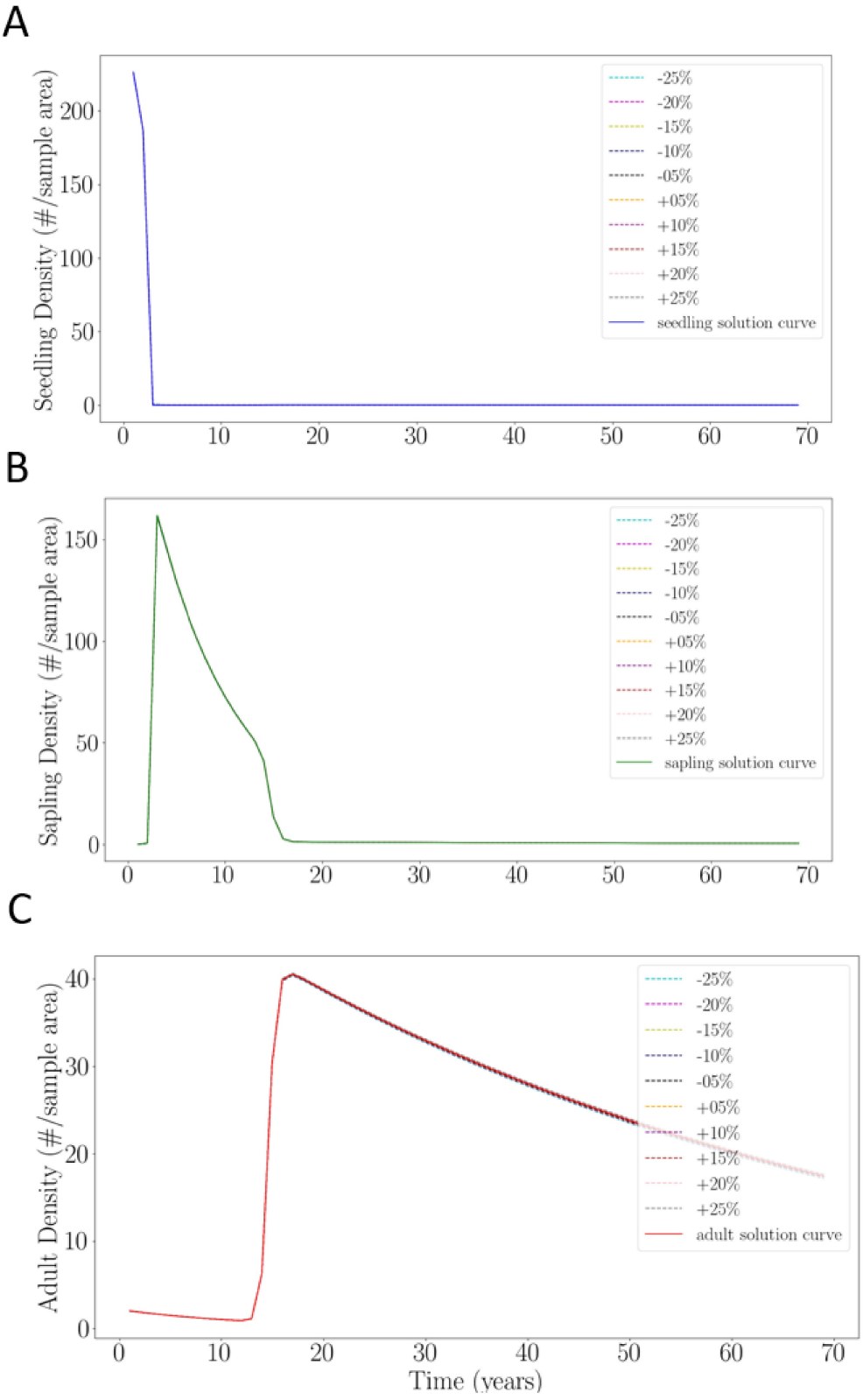

Figure B.4: Coefficient sensitivity results for the seedling (A), sapling (B), and adult (C) populations after perturbing the coefficient δ.

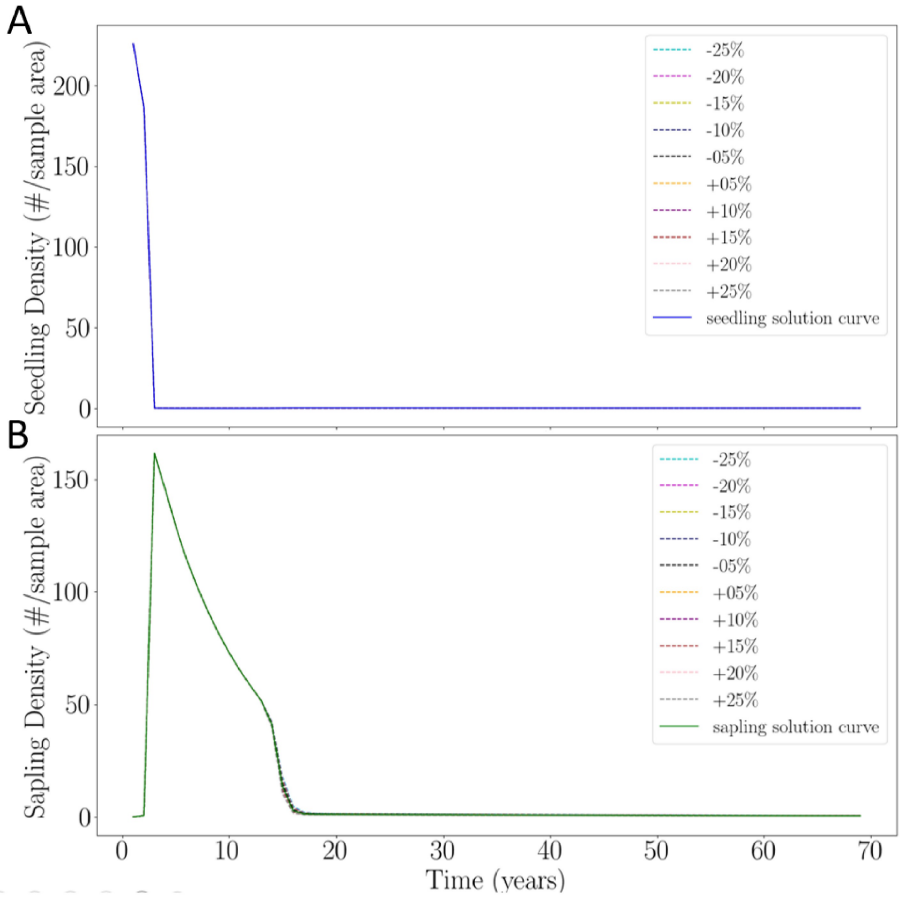

Figure B.5: Coefficient sensitivity results for the seedling population (A) and sapling population (B) after perturbing the coefficient σ.

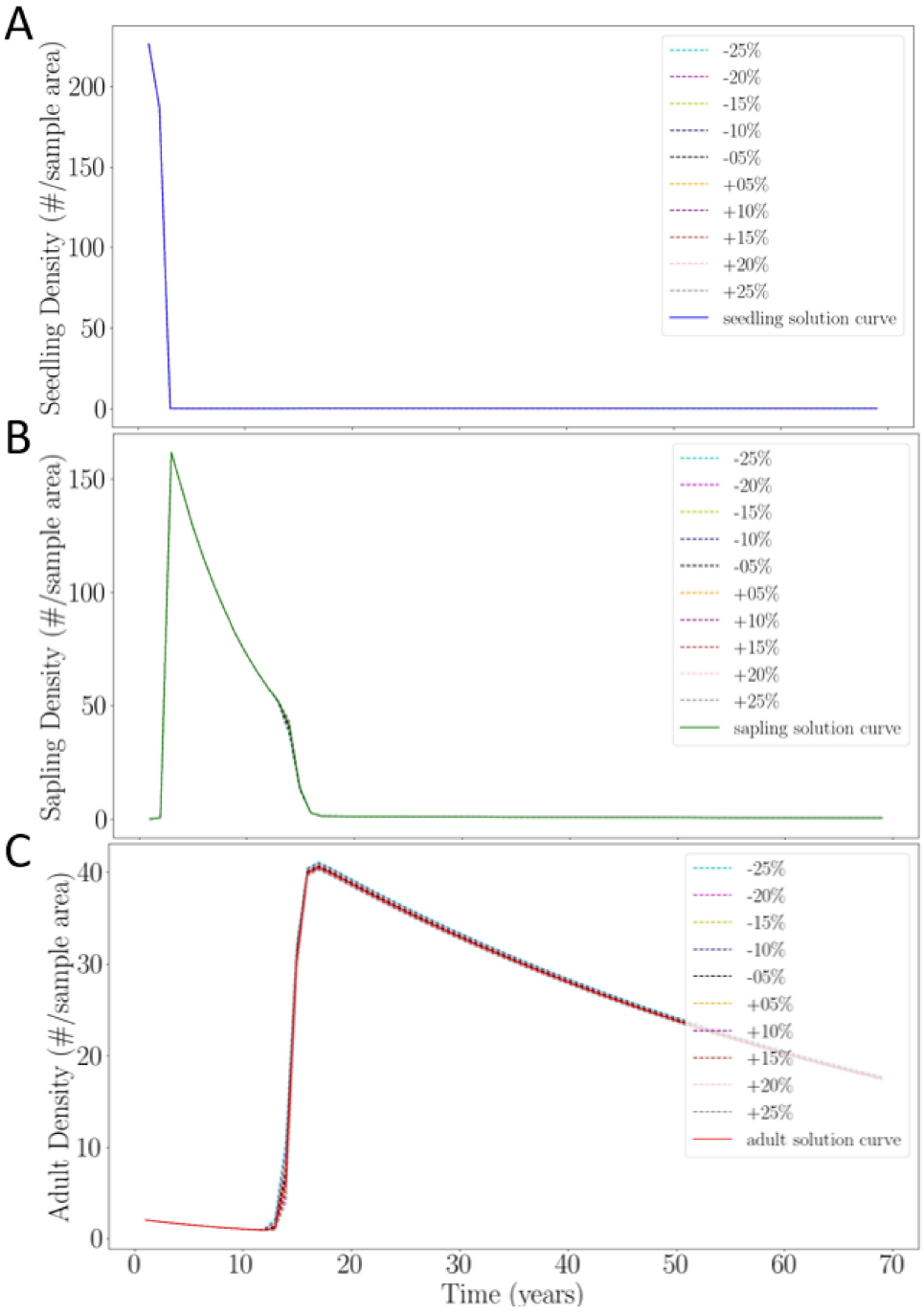

Figure B.6: Coefficient sensitivity results for the seedling (A), sapling (B), and adult (C) populations after perturbing the coefficient ψ.

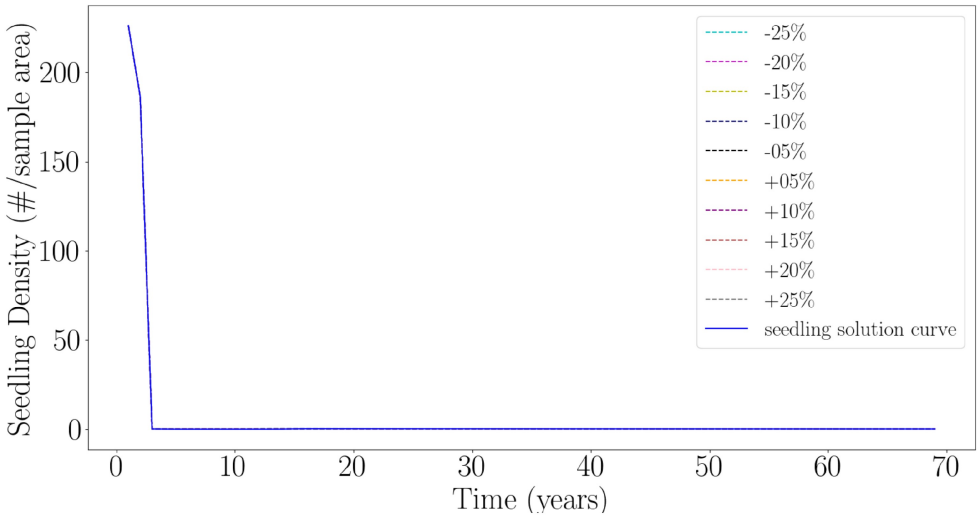

Figure B.7: Coefficient sensitivity results for the seedling population after perturbing coefficient t_{c_2}.

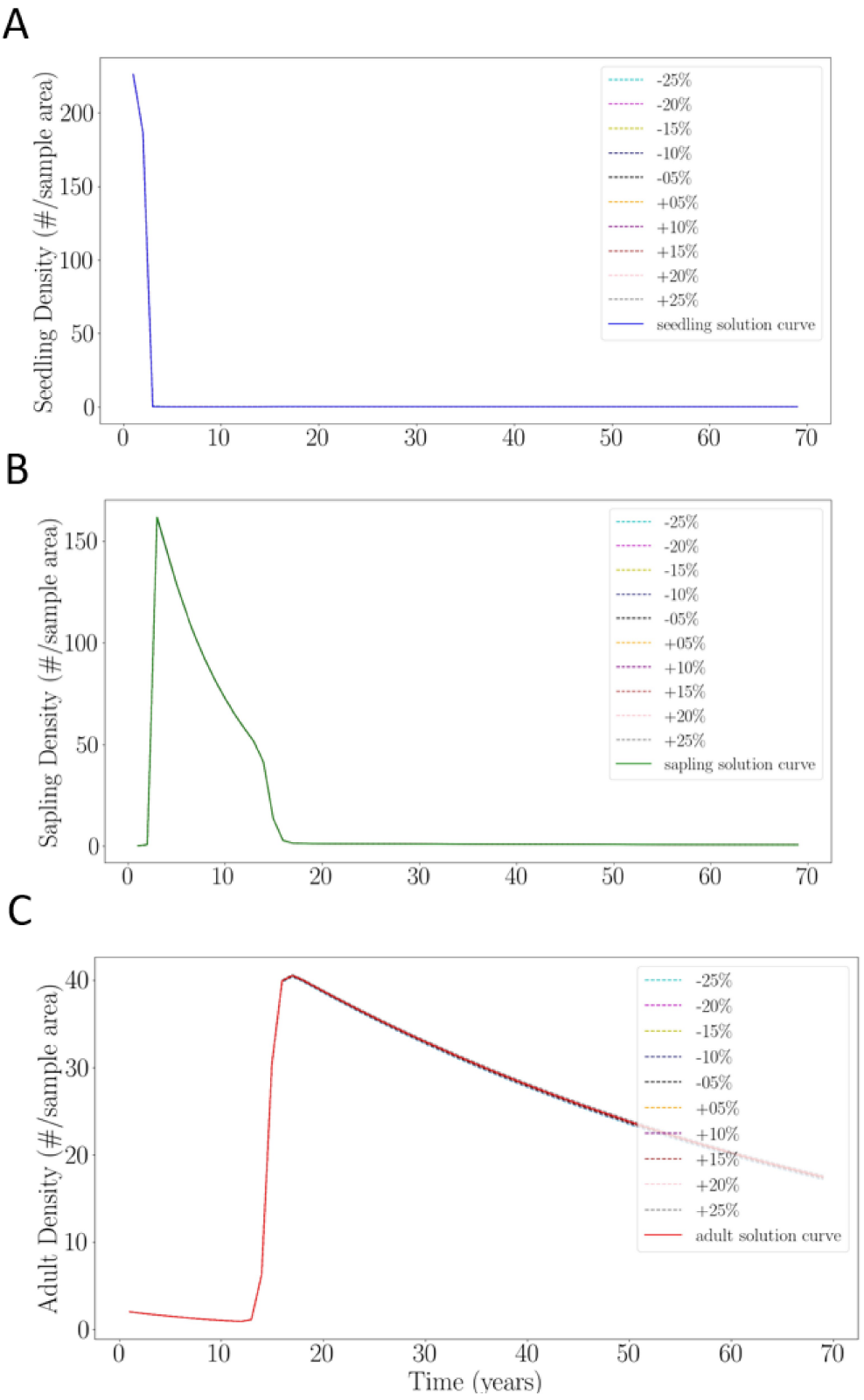

Figure B.8: Coefficient sensitivity results for the seedling (A), sapling (B), and adult (C) populations after perturbing the coefficient ζ.

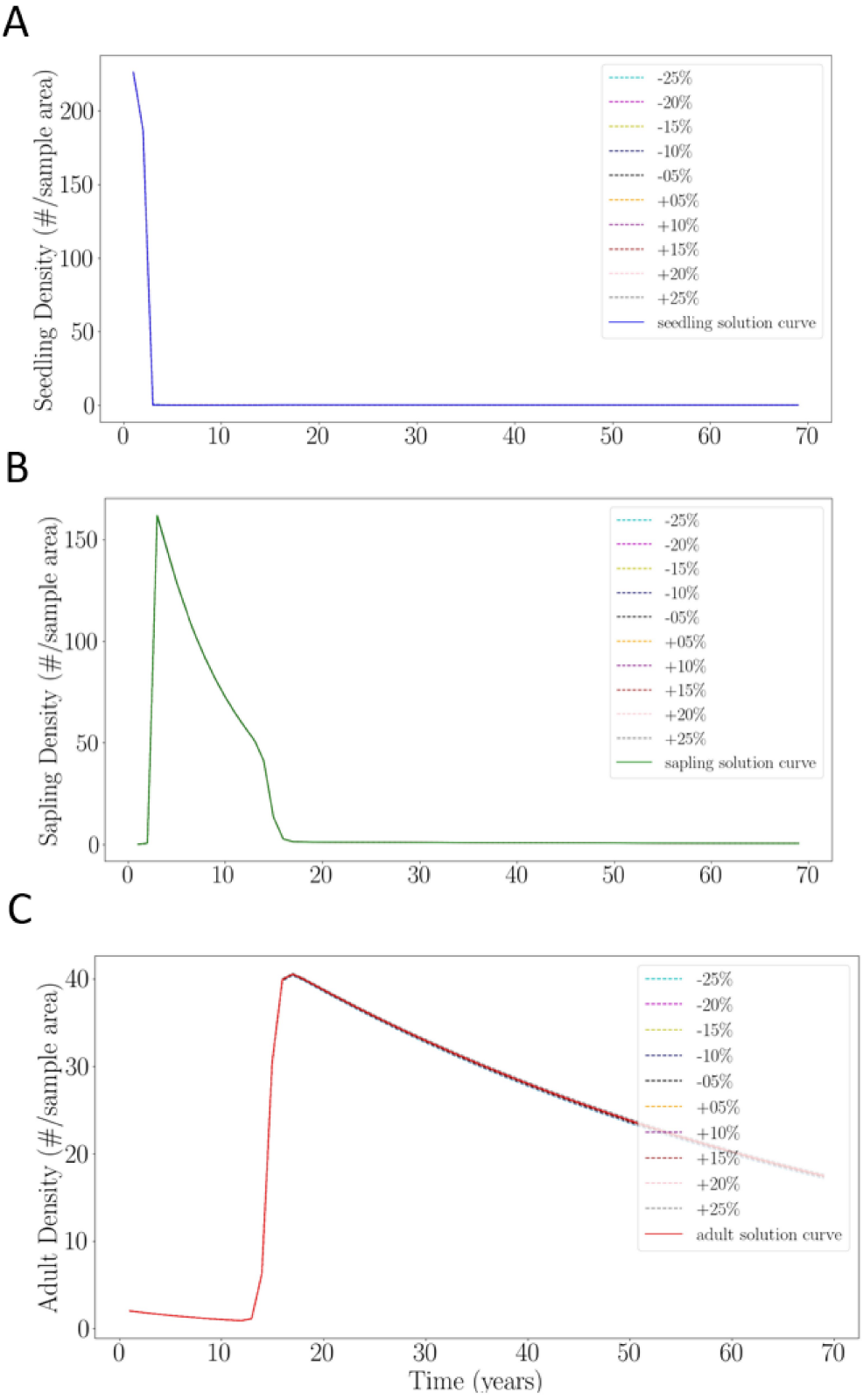

Figure B.9: Coefficient sensitivity results for the seedling (A), sapling (B), and adult (C) populations after perturbing the coefficient f.

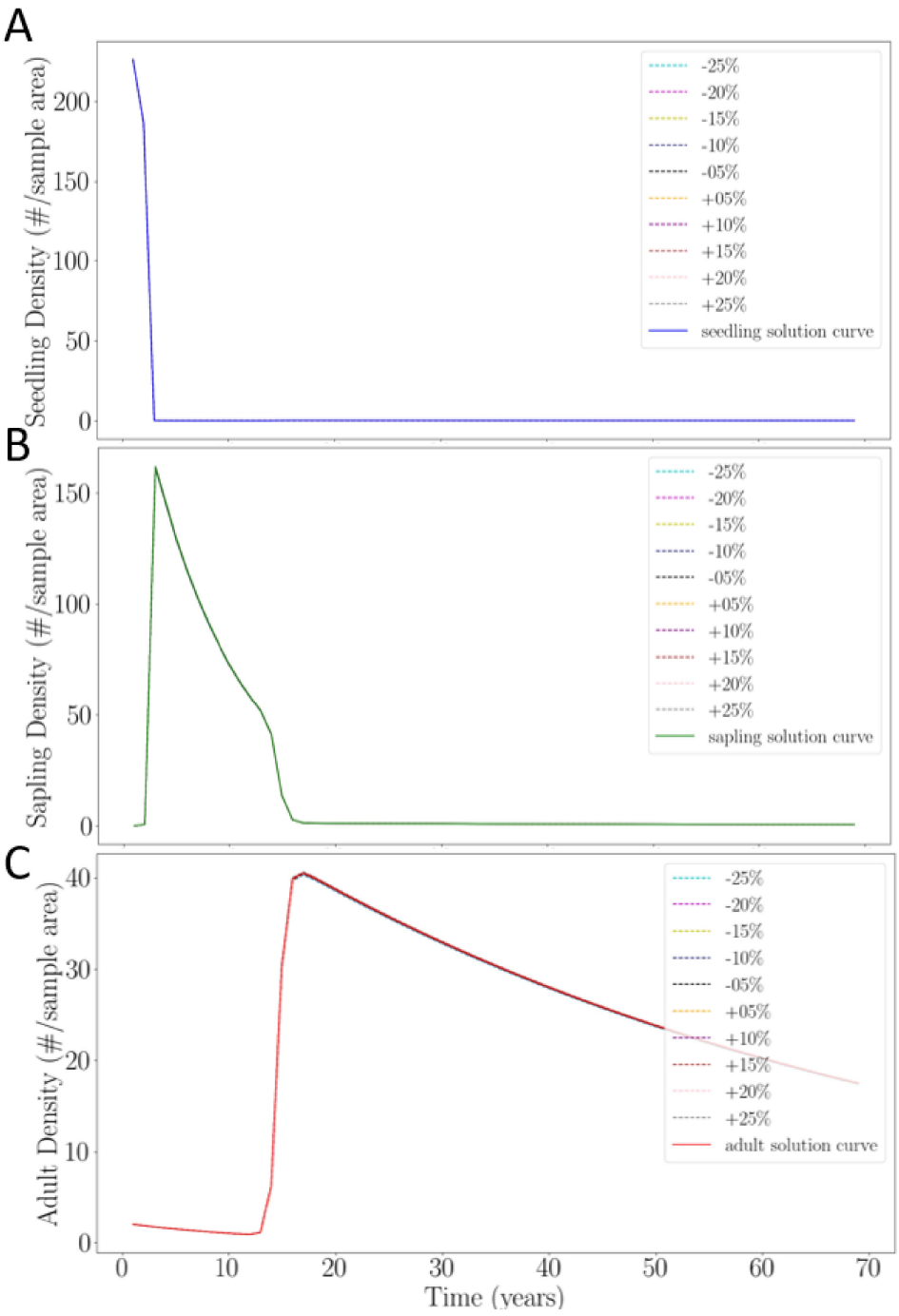

Figure B.10: Coefficient sensitivity results for the seedling (A), sapling (B), and adult (C) populations after perturbing coefficient g.

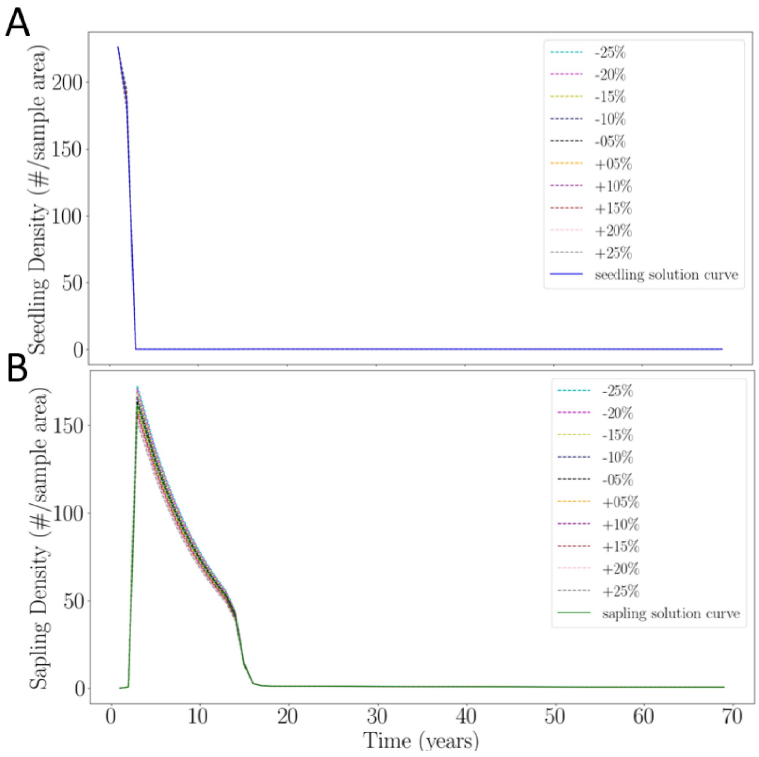

Figure B.11: Coefficient sensitivity results for the seedling population (A) and sapling population (B) after perturbing the coefficient h.

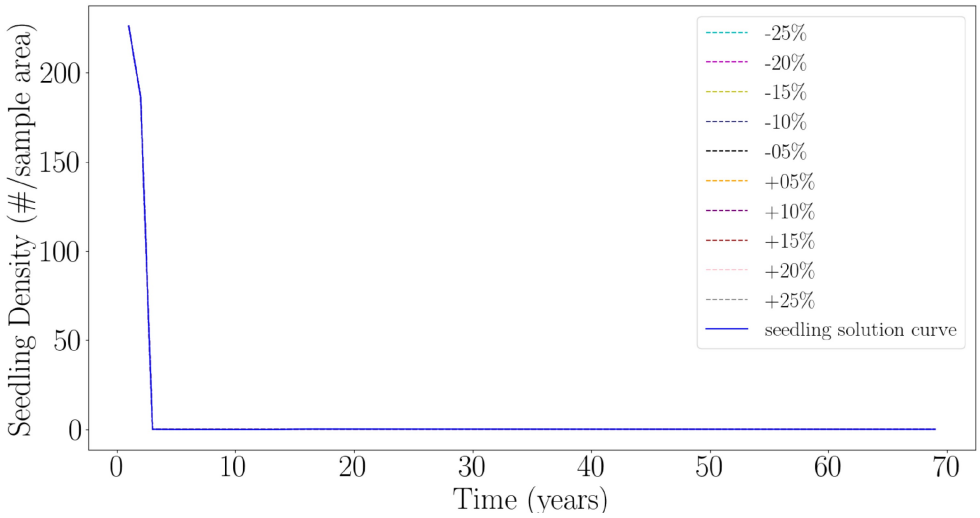

Figure B.12: Parameter sensitivity results for the seedling population after perturbing the parameter μ_2.

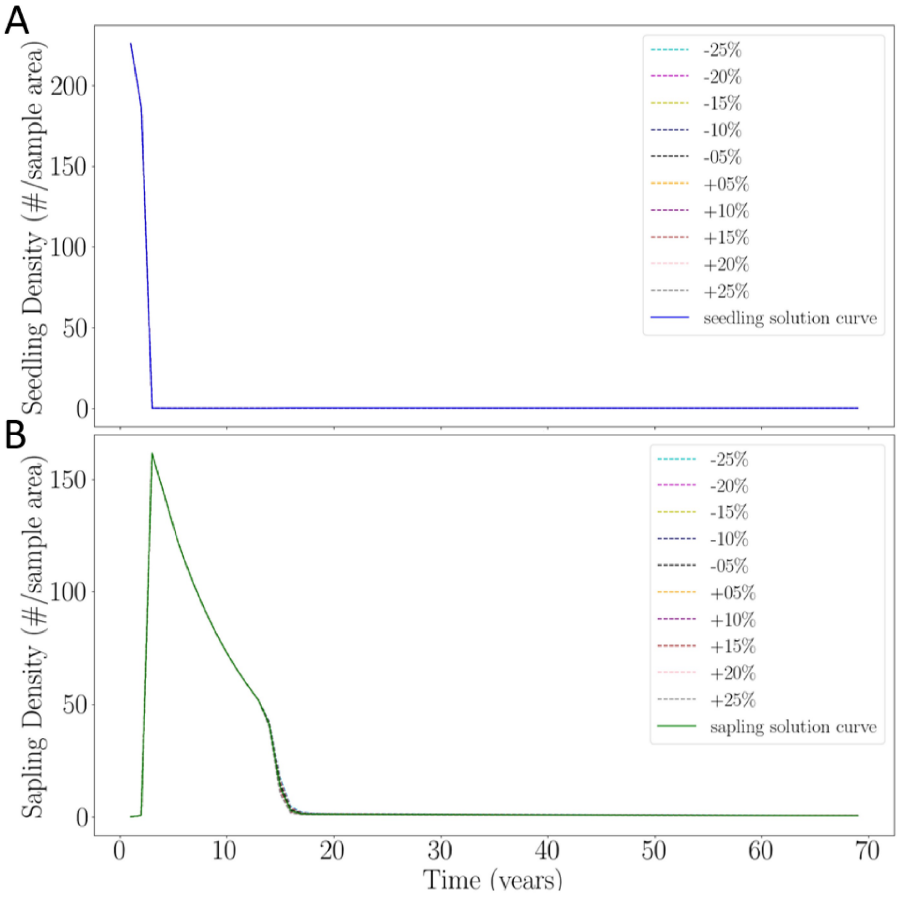

Figure B.13: Parameter sensitivity results for the seedling population (A) and sapling population (B) after perturbing the parameter μ_3.

B.2 Structure Sensitivity Analysis

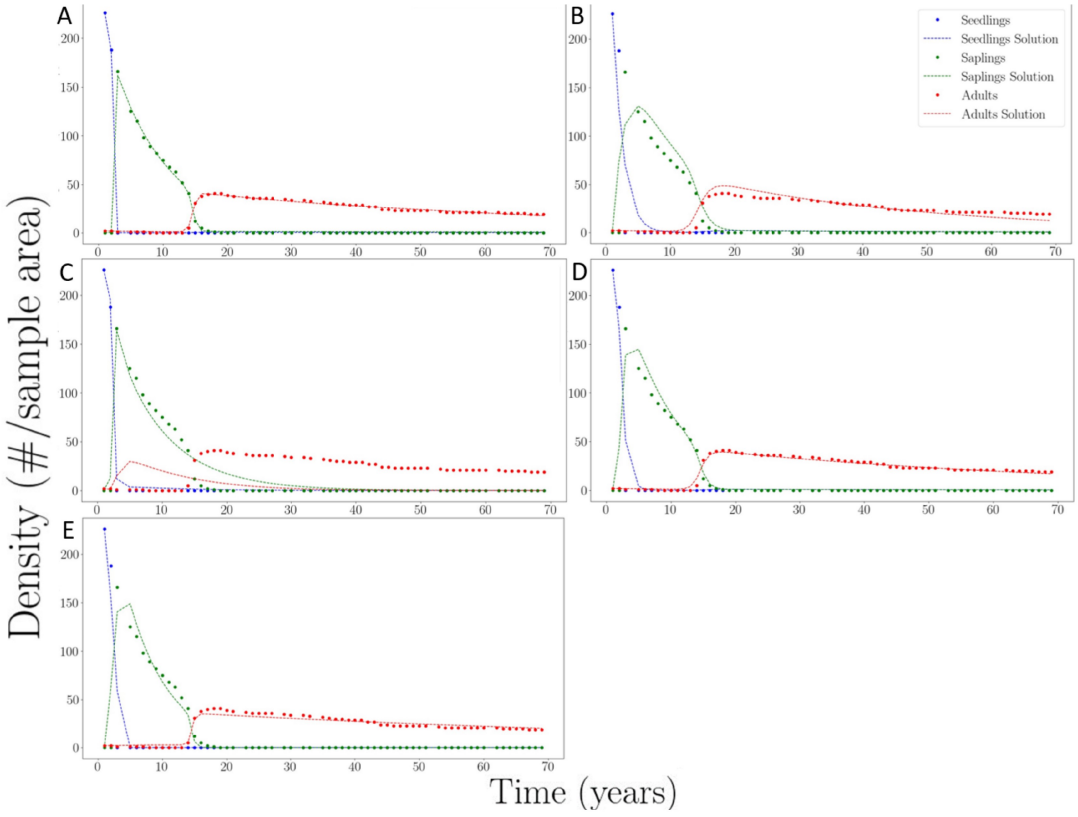

Figure B.14: Model 7 solution curves following the replacement of the coefficients δ (A), t_{c_1} (B), t_{c_2} (C), α (D), and γ (E).

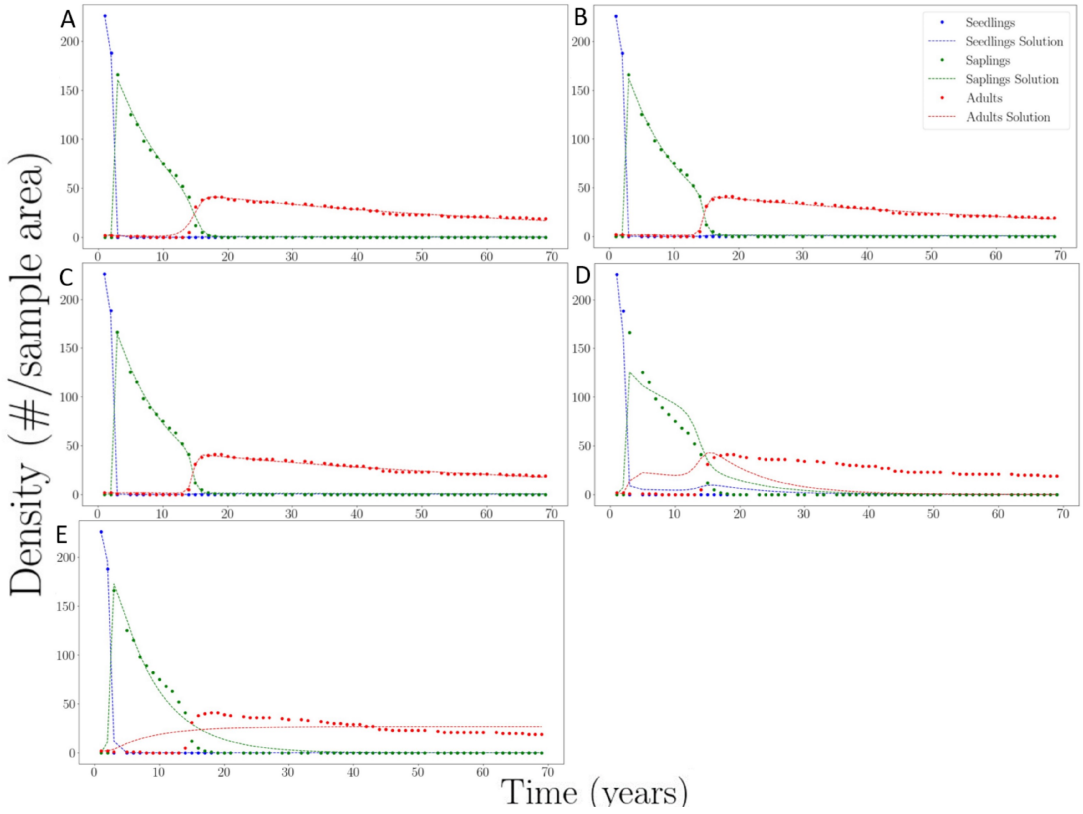

Figure B.15: Model 7 solution curves following the replacement of the coefficients and parameters ψ (A), f (B), h (C), μ_2 (D), and μ_3 (E).

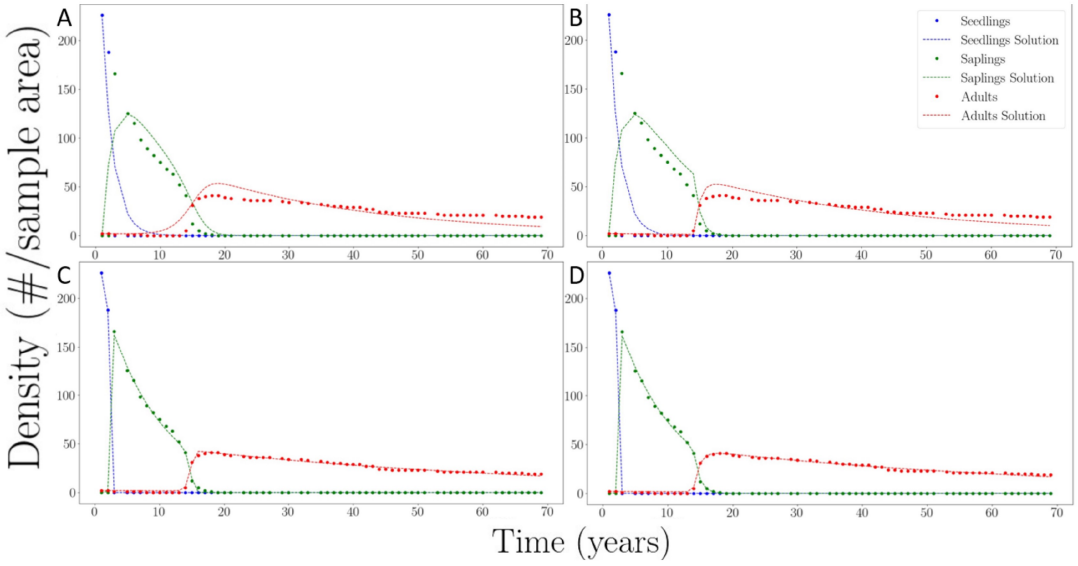

Figure B.16: Model 7 solution curves following the replacement of the coefficients β, ζ, σ, and g (A), β, ζ, and σ (B), β, ζ, and g (C), and ζ and g (D).